VILNIUS UNIVERSITY
FACULTY OF CHEMISTRY AND GEOSCIENCES
INSTITUTE OF CHEMISTRY
DEPARTMENT OF ANALYTICAL AND ENVIRONMENTAL CHEMISTRY

Hanna Klipan
Pharmaceutical Chemistry
Master's Thesis

LOW-TEMPERATURE SYNTHESIS AND CHARACTERIZATION OF MAGNESIUM AND MANGANESE WHITLOCKITE

Scientific advisor
Assist. Prof. Dr. Aleksej Žarkov

_____

Vilnius 2022

TABLE OF CONTENTS

ABBREVIATIONS

ACP – amorphous calcium phosphate;

ATP – adenosine triphosphate;

BCP – biphasic calcium phosphate;

BET – Brunauer-Emmett-Teller surface area analysis;

BSE – bovine spongiform encephalopathy;

CaP – calcium phosphates;

CDHA – calcium-deficient hydroxyapatite $Ca_{10}(PO_4)_6(OH)_2$;

CNC − computer numerical control;

DCPA – anhydrous dicalcium phosphate $CaHPO_4$;

DCP – monetite $CaHPO_4$;

DCPD – calcium hydrogen phosphate dihydrate $CaHPO_4 \cdot 2H_2O$;

DNA – deoxyribonucleic acid;

EXAFS – extended X-ray absorption fine structure;

FBP – β-fructose-1,6-diphosphate;

FTIR – Fourier-transform infrared spectroscopy;

FWHM – peaks width at half height;

HAp – calcium hydroxyapatite $Ca_{10}(PO_4)_6(OH)_2$;

NMR – nuclear magnetic resonance spectroscopy;

ICP-OES – inductively coupled plasma atomic emission spectroscopy;

MCP – monocalcium phosphate $Ca(H_2PO_4)_2$;

Mg-WH – magnesium whitlockite $Ca_{18}Mg_2(HPO_4)_2(PO_4)_{12}$;

Mn-WH – manganese whitlockite $Ca_{18}Mn_2(HPO_4)_2(PO_4)_{12}$;

SBF – simulated body fluid;

SEM – scanning electron microscope;

OCP – octacalcium phosphate $Ca_8(HPO_4)_2 (PO_4)_4 \cdot 5H_2O$;

PMMA – polymethyl methacrylate;

TCP – tricalcium phosphate $Ca_3(PO_4)_2$;

TTCP – tetracalcium phosphate $Ca_4(PO_4)_2O$;

TGA – thermogravimetric analysis;

WH – whitlockite;

XPS – X-ray photoelectron spectroscopy;

XRD – X-ray diffraction.

INTRODUCTION

The prevalence of disorders that cause bones to weaken, brittle, and fracture is expected to skyrocket as the population ages. Osteoporosis and brittle fractures are truly considered to be a costly human and socioeconomic burden throughout the world.

There has been significant progress in the development of biomedical materials in recent decades, including numerous ceramic materials for bone repair and reconstruction. Calcium phosphates (CaP) are considered to be quite promising substances in the field of bone regeneration due to their elemental makeup and structural similarity to natural bone tissue. Additionally, (CaP) bioceramics have demonstrated biocompatibility, osseointegration, and osteoconduction capabilities, which set them apart from other materials.

Magnesium whitlockite (Mg-WH, $Ca_{18}Mg_2(HPO_4)_2(PO_4)_{12}$) is a biologically important mineral in the living bone and a promising candidate in the field of regenerative medicine. This material is renowned for its exceptional biocompatibility and osteogenic potential. Mg ions in natural whitlockite stabilize its structure and endow the mineral with valuable biological properties. It was also observed that substitution of calcium with Mn ions can improve such properties as bone resorption control, cell adhesion promotion, and extracellular matrix protein production.

Thus, Mg and Mn ions might enhance the material's biological characteristics and make it more desirable for medical applications. As a result, there is a particular need to create a simple, cost-effective, and reliable WH synthesis approach that allows the preparation of a high-phase-purity product while also allowing the regulation of the amounts of Mg^{2+} and Mn^{2+} ions in the crystalline structure. Meanwhile, there is a scarcity of scientific data on Mn^{2+}-containing compounds with the WH structure. The lack of this information provides additional motivation for this work. In addition, the synthesis of CaP at low temperatures becomes a particularly important challenge because human bone tissue is formed under mild conditions from low-crystallinity CaP.

The main goal of this work was to investigate the synthesis process of magnesium and manganese whitlockites. For this purpose, the following objectives were set:
- to synthesize pure-phase Mg-WH and investigate its thermal stability;
- to develop a low-temperature synthesis technique for Mn-WH;
- to study the chemical composition, phase purity, and structural and morphological features of synthesized WH powders.

LITERATURE REVIEW

1.1 Calcium phosphates

Calcium phosphates are the most important inorganic constituents of biological hard tissues. In the form of carbonated hydroxyapatite (HAp), they are present in bone, teeth, and tendons to give these organs stability, hardness, and function [1]. Calcium phosphate crystals are also found in dead nature as mineral deposits of considerable size, having grown over many years under sometimes extreme conditions of pressure and temperature [2]. These compounds can be found in non-living nature in mineral deposits, sedimentary rocks (phosphorites), and, in rare cases, volcanic rocks (fluorapatite) (Fig. 1). In contrast, biologically formed calcium phosphates are often nanocrystals that are precipitated under mild conditions (ambient pressure, near room temperature) [3].
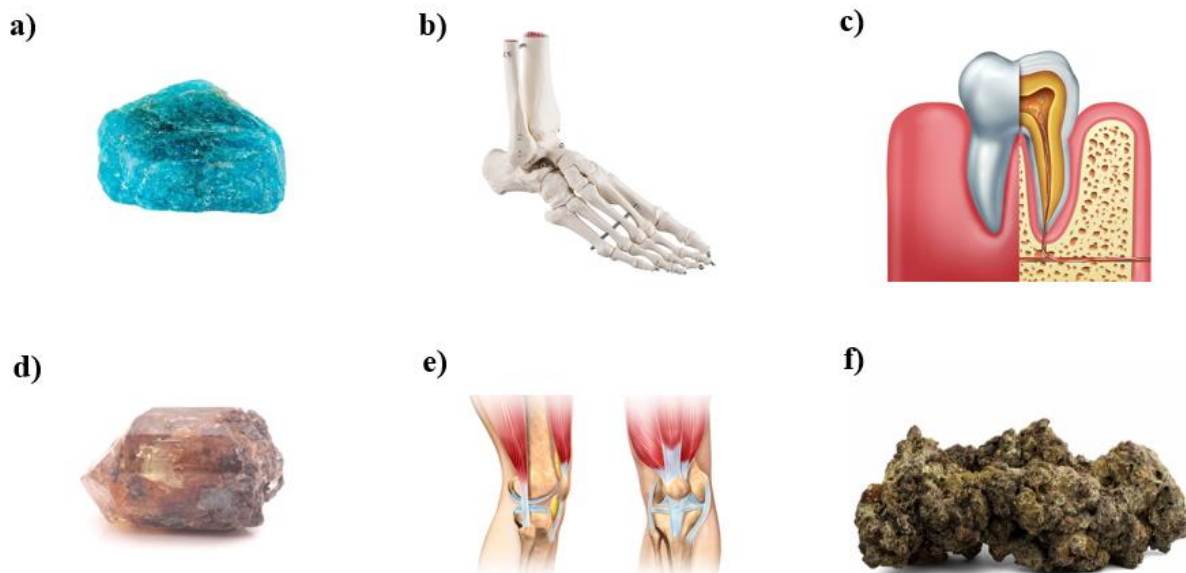

Fig. 1. The prevalence of CaP in living and non-living nature: a) Calcium phosphates in forms of fluorapatite found in volcanic rocks; b) Calcium phosphate is found in considerable amounts in bone tissue; c) The hardest substance in the human body, dental enamel, is made up of many minerals, including hydroxyapatite; d) Apatite found in mineral deposits; e) Hydroxyapatite deposits have been documented in many tendons remote from joints; f) Phosphorites deposits in sedimentary rocks.

The biological formation of minerals by living organisms is commonly called biomineralization. More than 60 minerals have been identified as being employed by living organisms for a variety of purposes, including protection (shell), tools (teeth), gravity sensors

(otoconia or statoliths), and skeletons (otoconia or statoliths). In terms of absolute quantity, calcium phosphates are minor in comparison to calcium carbonate ($CaCO_3$) and silicon dioxide ($SiO_2 \cdot nH_2O$), which are both abundant in marine single-cell organisms in large amounts [4].

Calcium phosphates are particularly essential in biomedicine since they are found in vertebrates (such as humans), as many diseases are caused by anomalies in the skeletal system (i.e., bone) or the dental system (in teeth). It must also be stressed that, although the presence of calcium phosphate in these hard tissues is crucial for survival, there are cases in which calcium phosphate minerals crystallize irregularly in undesired regions. These phenomena are called pathological crystallization or ectopic mineralization, of which atherosclerosis, stone formation, or dental calculus are prominent examples [5].

Because calcium phosphates make up the majority of the inorganic bone matrix, they can be used for bone regeneration or to aid the usage of other biomaterials. As a result, it is widely employed in a variety of applications and is constantly being researched.

1.1.1 Mineral phases of calcium phosphates

Calcium phosphates are found in a variety of chemical compositions and crystalline forms. The compound formed is determined by a variety of parameters, including temperature, pH, and impurities in the reaction mixture [6]. As various stoichiometric calcium phosphates are known, abbreviations have traditionally been introduced to distinguish between the different compounds. The molar Ca/P ratio and solubility are considered to be crucial parameters. For the chemically pure compounds, the Ca/P ratio can be between 0.5 ± 2.0. In general, the lower this ratio, the more acidic and soluble in water the calcium phosphate is [7].

MCPM (monocalcium phosphate monohydrate, $Ca(H_2PO_4)_2 \cdot H_2O$) is the most acidic and water-soluble calcium phosphate compound. It precipitates from highly acidic solutions that are normally used in the industrial production of phosphorus-containing fertilizer („triple superphosphate"). At temperatures above 100 °C, it transforms into MCPA (monocalcium phosphate anhydrate, $Ca(H_2PO_4)_2$). Because of its comparatively high acidity and solubility, MCPM is never found in biological calcifications. However, MCPM is used in some calcium phosphate cement in medicine. Other applications are as antacids, acidulants, and mineral supplements for baking powders, foods, and beverages [8].

MCPA is the anhydrous form of MCPM. It crystallizes under similar conditions as MCPM but at temperatures above 100 °C (e.g. from highly concentrated mother liquors in fertilizer production). MCPA, like MCPM, does not present in calcified tissues and has no contemporary medical applications; however, it is well-known as a fertilizer [9].

DCPD (dicalcium phosphate dihydrate, $CaHPO_4 \cdot 2H_2O$; the mineral brushite) can be easily crystallized from aqueous solutions. DCPD transforms into dicalcium phosphate anhydrate at temperatures above 80 °C. DCPD is of biological importance because it is often found in pathological calcifications (dental calculi, crystalluria, chondrocalcinosis, and urinary stones). DCPD has been proposed as an intermediate in bone mineralization and enamel dissolution in

acids (dental caries). In surgery, DCPD is used in calcium phosphate cement and, in dentistry, in toothpaste together with fluoride-containing compounds (e.g. NaF) for protection against caries. Other applications include fertilizers, glass manufacture, calcium supplements in meals, and mineral supplements in cereals [10].

DCPA (dicalcium phosphate anhydrate, $CaHPO_4$; the mineral monetite) is the anhydrous form of DCPD. DCPA, like DCPD, can be crystallized from aqueous solutions but at 100 °C. Unlike DCPD, DCPA occurs in neither normal nor pathological calcifications. DCPA is utilized in calcium phosphate cement and polishing agents, calcium and phosphate sources in nutritional supplements, tableting aids, and toothpaste components [11].

OCP (octacalcium phosphate, $Ca_8(HPO_4)_2(PO_4)_4 \cdot 5H_2O$) is often found as an intermediate phase during the precipitation of the thermodynamically more stable calcium phosphates (e.g. HA, calcium-deficient HA (CDHA)) from aqueous solutions. OCP consists of apatite layers (with atomic arrangements of calcium and phosphate ions similar to those of HA) separated by hydrated layers (water molecules). OCP is of great biological importance because it is one of the stable components of human dental and urinary calculi. It is essential for the in vivo formation of apatite biominerals. Although OCP has not been observed in vascular calcifications, it has been strongly suggested that it is the precursor phase to the biological apatites present in natural and prosthetic heart valves [12].

β-TCP (β-tricalcium phosphate) is the „true calcium orthophosphate" of the stoichiometric composition $Ca_3(PO_4)_2$. It cannot be precipitated from solution, but may only be prepared by calcination, e.g. of CDHA, at temperatures above 800 °C. At temperatures above 1125 °C, it transforms into the high-temperature phase α-TCP. Being the stable phase at room temperature, β-TCP is less soluble in water than α-TCP. Pure -TCP never occurs in biological calcifications. Only the magnesium-containing form called whitlockite (chemical formula: $(Ca, Mg)_3(PO_4)_2$) is found in dental calculi and urinary stones, dental caries, salivary stones, arthritic cartilage, as well as in some soft-tissue deposits. In biomedicine, β-TCP is used in calcium phosphate bone cement. In combination with HA, β-TCP is used as a „biphasic calcium phosphate" (BCP) as a bone-substitution ceramic. Other applications include fertilizers, polishing, dental powders, porcelains, pottery, enamel, and animal food supplements [13].

α-TCP (α-tricalcium phosphate, $Ca_3(PO_4)_2$) is a metastable phase at room temperature, prepared from β-TCP at above 1125 °C. α-TCP is more reactive in aqueous systems than β-TCP and can be hydrolyzed to a mixture of other calcium phosphates. It never occurs in biological calcifications and has a limited application in medicine in calcium phosphate cement α-TCP is also used as a fertilizer [14].

ACP (amorphous calcium phosphate) is often encountered as a transient phase during the formation of calcium phosphates in aqueous systems. Usually, ACP is the first phase that is precipitated from a supersaturated solution prepared by rapid mixing of solutions containing calcium cations and phosphate anions. The chemical composition of ACP strongly depends on the solution pH value and the concentrations of calcium and phosphate ions in the mother liquor. For

example, ACP phases with Ca/P ratios in the range of 1.18:1 (precipitated at solution pH 6.6) to 1.53:1 (precipitated at solution pH = 11.7) and even up to 2.5:1 have been described [15].

The structure of ACP is still uncertain. IR spectra of ACP show broad, featureless phosphate absorption bands. The compounds are amorphous, according to X-ray diffraction experiments. Electron microscopy of ACP usually reveals spherical particles with typical diameters of 20 ± 200 nm. However, ACP likely has an apatite short-range structure, but with a crystal size so small that it appears amorphous in X-ray diffraction experiments (no coherent X-ray scattering). This is supported by X-ray absorption spectroscopic data (EXAFS; extended X-ray absorption fine structure) on biogenic and synthetic samples. On the other hand, it was proposed that the basic structural unit of ACP is a 9.5 Å diameter, roughly spherical cluster of ions with the composition $Ca_9(PO_4)_6$. These clusters were found experimentally as seed nuclei during the crystallization of HA, and a model was developed to describe the crystallization of HA as a stepwise assembly of these units. Biologically, ACP (often containing magnesium, carbonate, and pyrophosphate) is found in soft-tissue pathological calcifications (e.g. heart-valve calcifications of uremic patients). In medicine, ACP is sometimes used in calcium phosphate cement. Bioactive composites of ACP with polymers have properties suitable for use in dentistry and surgery [16].

CDHA (calcium-deficient hydroxyapatite) can be easily prepared by the simultaneous addition of calcium- and phosphate-containing solutions into boiling water, followed by boiling the suspension for several hours. During this time, initially precipitated OCP or ACP (this depends on the solution pH value) are transformed into CDHA. On heating above 700 °C, dry CDHA with Ca/P = 1.5:1 will convert into β-TCP, and that with 1.5:1 < Ca/P < 1.67:1 will convert into a mixture of HA and β-TCP (the above-mentioned biphasic calcium phosphate, BCP). Because of its nonstoichiometric character, CDHA always contains other ions. The extent depends on the counterions of the chemicals used for preparation (e.g. Na^+, Cl^-). There have been no direct determinations of the structures of CDHA and the unit cell parameters are uncertain. As a first approximation, CDHA may be considered as HA with some ions missing. Unsubstituted CDHA (i.e. containing calcium, phosphate, hydrogen phosphate, and hydroxide ions only) does not exist in biological systems; it occurs only with ionic substitutions: Na^+, K^+, Mg^{2+}, Sr^{2+} for Ca^{2+}; carbonate for phosphate; fluoride, chloride, and carbonate for hydroxide, and some water, form the so-called „biological apatite" or dahllite – the main inorganic component of animal and human normal and pathological calcifications. Therefore, CDHA is a very promising compound for the manufacture of artificial bone substitutes [17].

HA (hydroxyapatite, $Ca_{10}(PO_4)_6(OH)_2$) is the most stable and least soluble of all calcium orthophosphates. Pure HA crystallizes in the monoclinic space group *P2₁/b*. However, at temperatures above 250 °C, there is a monoclinic to hexagonal phase transition in HA (space group *P6₃/m*). Some impurities, like partial substitution of hydroxide by fluoride or chloride ions, stabilize the hexagonal structure of HA at ambient temperature. For this reason, the very rare single crystals of natural HA always exhibit a hexagonal space group [18].

HA can be prepared in aqueous solutions by mixing exactly stoichiometric quantities of calcium- and phosphate-containing solutions at pH = 9, followed by boiling for several days under

a CO_2-free atmosphere, filtration, and drying. Microcrystalline samples of HA can also be prepared by solid-state reactions of other calcium phosphates (e.g. MCPM, DCPA, DCPD, OCP) with CaO, $Ca(OH)_2$, or $CaCO_3$ at temperatures above 1200 °C, in an atmosphere of equal volumes of water and nitrogen. Single crystals of HA can be prepared by hydrothermal synthesis. A water-free synthesis can be performed in ethanol from $Ca(OEt)_2$ and H_3PO_4. Pure HA never occurs in biological systems. However, because of the chemical similarities to bone and teeth minerals (, HA is widely used as a coating for orthopedic (e.g. hip-joint prosthesis) and dental implants, and a calcium phosphate cement with HA has also been developed. Because of its great similarity to bone minerals, HA is also used in the liquid chromatography of proteins and other biological compounds [19].

TTCP (tetracalcium phosphate $Ca_4(PO_4)_2O$) is the most basic calcium orthophosphate. However, its solubility in water is higher than that of HA. TTCP cannot be precipitated from aqueous solutions, and thus can only be prepared by a solid-state reaction above 1300 °C, for example, by heating homogenized equimolar quantities of DCPA and $CaCO_3$ in dry air, or a stream of dry nitrogen. TTCP is not very stable in aqueous solutions; it slowly hydrolyses to HA and calcium hydroxide. Consequently, TTCP is never found in biological calcifications. In medicine, TTCP is widely used for the preparation of various self-setting calcium phosphate cement [20].

Whitlockite (WH) is the low-temperature phase of calcium phosphate formed in aqueous solutions in the presence of Mg^{2+} ions. The structure of whitlockite is very similar to β-TCP, however, there's a significant difference in the chemical composition and properties of these substances. Despite the rare distribution of whitlockite in nature, it is one of the major components in human bone tissue. For more information on WH, see 1.4. subsection [21].

1.1.2 Applications of calcium phosphates

Medical intervention is frequently required for the treatment of injuries or disorders. Biomaterials have been progressively used to improve surgical operations or to restore lost function throughout the last 50 years [22]. Bone fractures are typically repaired with metallic wires, nails, screws, and plates, joints are replaced with artificial endoprostheses (hip or knee), and missing teeth are replaced with metallic implants in the jaw, to name a few instances. When foreign materials come into contact with the body, the issue of biocompatibility becomes critical, as any unfavorable consequence (particularly toxicity, allergies, inflammation, corrosion, and mechanical failure) must be avoided at all costs. The hunt for optimally designed biomaterials continues as a collaborative endeavor by physicians, engineers, chemists, and physicists [23].

Calcium phosphates have great biocompatibility, which means they are well-accepted by the body and integrate well, for example, into the bone after implantation. This is due to their almost ubiquitous presence in the body, whether dissolved or solid. As a result, they have found significant applications as biomaterials, particularly in hard-tissue regeneration. In bulk, calcium phosphates are utilized by orthopedic and maxillofacial surgeons as an artificial bone-substitution material for surgical repair of bone abnormalities [24].

A bone defect produced, for example, by tumor extraction, a difficult fracture, or inflammation must be filled with an appropriate material to allow new bone to grow into the defect. Otherwise, fibrous tissue would infiltrate the defect and impede bone development. Because the ideal substitute (the "golden standard"), a patient's spongious bone from the Iliac crest (hip), is usually not available in sufficient quantities, and as materials of biological origin are being debated due to possible infections or immune reactions, the need for a fully synthetic material is obvious [25]. There are numerous calcium phosphate ceramics available on the market now for the treatment of bone deformities. Synthetic bone-substitution materials are typically chemically based on HA, β-TCP, or BCP (a mixture of HA and β-TCP). The following are typical requirements for a perfect substitute [26]:

• a porosity with pore diameters of about 100 μm (to allow bone cell ingrowth);

• a biodegradation rate corresponding to bone tissue formation (i.e. between a few months and around two years);

• appropriate mechanical stability.

Under physiological conditions, HA is more stable than α- and β-TCP due to its lower solubility and slower desorption kinetics. Implants of calcined HA with high crystallinity are present in a defect even years after implantation in a nearly identical form, hence β-TCP or BCP ceramics are preferred today. An optimal material should degrade inside the defect concurrently with the development of new bone, implying that the defect should be completely restored with biological material. Fig. 2 depicts three distinct calcium phosphate-based bone substitute materials. Implant porosity is critical for allowing cell invasion and bone ingrowth [27].
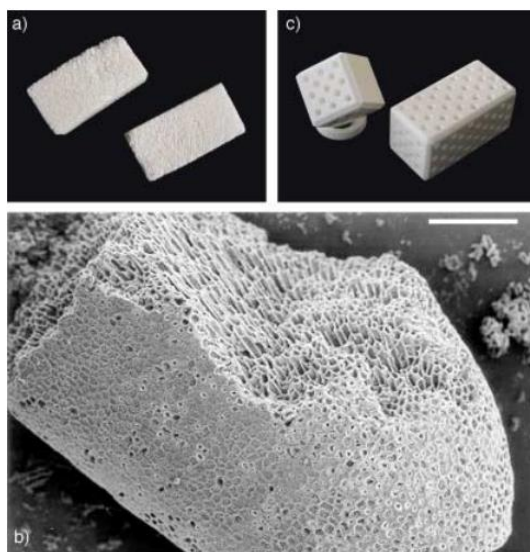

Fig. 2. Examples of porous calcium phosphate-based bone-substitution materials: a) Cerabone (HAp) from spongious calcined bovine bone (about $3 \times 1 \times 1$ cm^3); b) Algipore (HAp) from hydrothermal processing of calcium carbonate-containing algae with ammonium phosphate. Scale bar: 100 μm; c) Cerasorb (synthetic phase-pure β-TCP) with CNC (computer numerical control)-drilled holes (about $1 \times 1 \times 2$ cm^3) [2].

Bone cement based on calcium phosphates, which harden inside the defect, presented a new approach to the treatment of bone defects. Although there are several formulations available, they typically consist of solid calcium phosphates combined with a solution to induce the precipitation of a CDHA-like phase. The benefit of this approach is that the cement conforms to the fault geometry better than ceramic materials implanted as solids. Because the structure and composition of hardened calcium phosphate are similar to those of bone minerals, resorption is enhanced [5].

Metals with calcium phosphate coatings are frequently used in medicine. Endoprostheses (complete hip replacements) and artificial tooth sockets both use metallic implants. The mechanical stability criterion mandates the employment of a metallic body for such devices. Because metals typically do not undergo bone-bonding, that is, they do not form a mechanically stable link between the implant and bone tissue, methods to increase mechanical contact at the interface have been investigated. One option is to coat the metal with calcium phosphate ceramics, which roughen the bone surface and so improve bone bonding, and may thus act as a glue between the metal and bone (Fig. 3) [28].

Fig. 3. Calcium phosphates in hip endoprostheses: a ceramic ball joint (Al_2O_3), a calcium-phosphate coated endoprosthesis („cementless endoprosthesis"), and an uncoated endoprosthesis that must be fixed in place with PMMA bone cement [2].

Currently, two approaches to bone coating are used: high-temperature plasma spraying of molten calcium phosphate and precipitation from a supersaturated calcium phosphate solution. From a chemistry standpoint, the first method is rather rough. To create a uniform coating, solid calcium phosphate is poured into a plasma flame and directed towards an implant that is rotated correctly. This rapid quenching results in the production of a calcium phosphate combination on the implant surface. Following this technique, metal and calcium phosphate are tightly bonded [29].

The second method entails immersing metallic implants in supersaturated calcium phosphate solutions. This technology was heavily supported by the work of Kokubo and colleagues, as well as van Blitterswijk and colleagues, who demonstrated that after suitable surface etching, a stable interface between metal and ceramic emerges. The technology also allows for the coating of internal surfaces (which is difficult with plasma spraying) and the incorporation of biologically active molecules, such as proteins or antibiotics, into the coating. Surface coating with a biomimetic fault apatite by dipping into the simulated bodily fluid (SBF), a solution containing the inorganic ions of human blood plasma in near-natural quantities, is a specific instance [30].

Figure 3 shows both a calcium phosphate-coated and an uncoated hip endoprosthesis. The latter has to be fixed in the femur bone by a suitable bone cement based on poly(methylmethacrylate) (PMMA). Note that this polymer is not biodegradable and remains in the operation site [2]. The same principles are applicable to tooth implant systems that are surgically implanted into the jawbone and to which artificial teeth are affixed. In general, mechanical contact between implant and bone is critical because significant stresses must be endured. Coating such dental implants with calcium phosphates (often via plasma spraying) results in improved and faster bone adhesion. Fig. 4 represents a plasma-spray-coated dental implant under low and high magnification. It should be noted that this polymer is not biodegradable and hence remains at the operation site [2, 31].
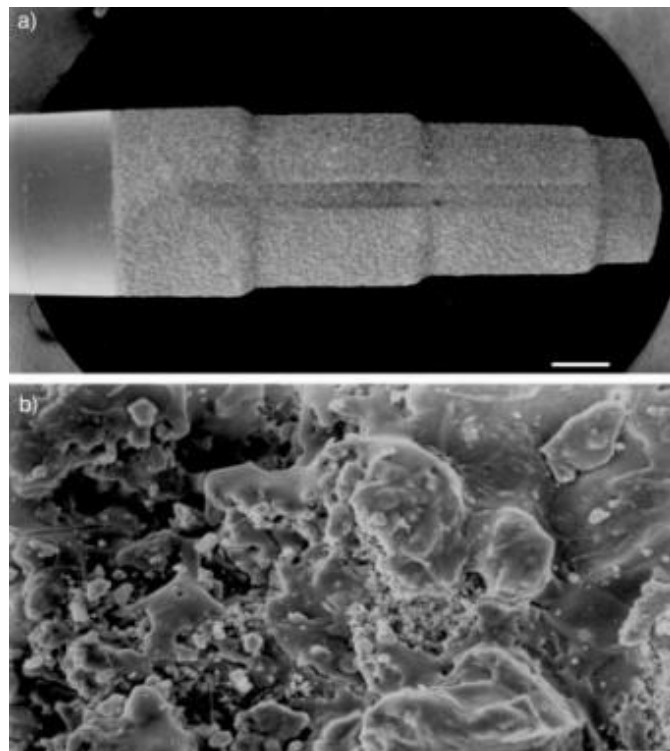

Fig. 4. Dental implants (by Friadent) coated with calcium phosphate by a plasma-spray process [2].

The same principles are valid for tooth implant systems that are fixed into the jawbone, onto which artificial teeth are attached. In general, the mechanical contact between implant and bone is

crucial, as considerable forces have to be withstood. Coating such dental implants with calcium phosphates (usually by plasma spraying) leads to better and faster bone attachment [32].

1.2 Metal-substituted calcium phosphates

Natural bone tissue has a high capacity for trace elements, which contribute to the tissue's remarkable properties. Synthetic calcium phosphates do not replicate the elemental and phase composition of natural bone tissue, and therefore the biological properties of these substances are inferior to those of natural bone tissue. Numerous researchers have focused on enhancing the mechanical properties of synthetic calcium phosphates. One of the strategies is to substitute calcium phosphates with ions present naturally in bone tissue such as Mg, Mn, Zn, and Si [33].

Biosorption is one of the most essential features of calcium phosphates used for bone regeneration, and it is directly dependent on the substance's solubility under biological conditions. The presence of various ions in the structure also influences the material's solubility, which can be enhanced or lowered due to the partial replacement of Ca^{2+} ions [34]. Partially replacing a substance with ions, which can give it antibacterial qualities, is especially relevant in the field of bone implants, since infections produced by the implantation process are a typical adverse effect. Incorporating antibacterial ions into the structure of the regeneration material itself can assist to prevent this and accelerate the healing process [35].

The incorporation of Mg^{2+} ions into the β-TCP structure diminishes the solubility of this substance under acidic conditions while increasing the solubility of HAP. Furthermore, Mg-substituted HAP has improved resorption and incorporation into bone tissue. The same trend may be seen for Si and HAp that have been partially changed by Bi^{3+} ions. The substitution with Cu^{2+}, Zn^{2+}, Mn^{2+}, Ag^{+} and Fe^{3+} ions into the β-TCP structure greatly improve the antibacterial properties of the material [36].

When HAP is substituted with Zn ions, it has been shown to limit the growth and multiplication of bacteria and fungus such as *E. coli, S. aureus, Candida albicans*, and *Streptococcus* mutants. HAp prevents the growth of germs on the surface of the enamel and minimizes the creation of dental calculus. HAP granules doped with Ag or Cu are non-cytotoxic and offer excellent antibacterial capabilities against a wide range of pathogens [18].

Those traces of ions can affect the lattice parameters, crystallinity, dissolution kinetics, and other physical properties of apatite. These metal enforcers are also considered to have a significant role in improving cell-material interactions of calcium phosphates and strengthening their mechanical properties. The process of cell interaction on materials is very dynamic, thus encouraging an exceptional tissue response at the surface of the biomaterial [16, 17].

Ion traces in apatite can impact its lattice parameters, crystallinity, dissolution kinetics, and other physical properties. These metal enforcers are also thought to play an important role in enhancing calcium phosphate cell-material interactions and boosting their mechanical characteristics. The process of cell interaction on materials is highly dynamic, stimulating an outstanding tissue response at the biomaterial's surface [37].

1.3 Biological roles of Mg and Mn in the human body

1.3.1 Biological role of magnesium in the human body

Magnesium is one of the most abundant elements in the human body. It is involved as a cofactor in more than 300 enzyme systems and is required for such fundamental processes as energy production, nucleic acid synthesis, blood glucose control, and blood pressure regulation. This element participates in the active transport of calcium and potassium ions across cell membranes, a process that is important to nerve impulse conduction, muscle contraction, and normal heart rhythm [38].

Approximately 67% of Mg in the human body is stored in bone tissues, and 30% is exchangeable on the crystal surface of the bone, providing a dynamic supply for maintaining intra- and extracellular Mg concentrations. Bone surface Mg levels are related to serum Mg. Accordingly, surface bone Mg increases with Mg loading, as described in chronic renal disease. The larger fraction of bone Mg is probably deposited as an integral part of the apatite crystal and its release follows the resorption of bone [39].

It has been revealed that magnesium ions (Mg^{2+}) affect the overall rate of seeded calcium phosphate crystallization and the subsequent growth of hydroxyapatite (HA). Moreover, as a participant, Mg^{2+} induces osteogenic differentiation and osteoblast differentiation, which occur with the use of degradable magnesium metals and alloys, thereby promoting bone regeneration [40].

Apart from a structural role in the crystals, Mg is essential to all living cells, including osteoblasts and osteoclasts. Intracellularly, Mg is vital for numerous physiological functions. First of all, Mg is fundamental for ATP, the main source of energy in the cells. Moreover, Mg is a cofactor of hundreds of enzymes involved in lipid, protein, and nucleic acid synthesis. Because of its positive charge, Mg stabilizes cell membranes. It also antagonizes calcium and functions as a signal transducer. It is therefore not surprising that alterations of Mg homeostasis impact cell and tissue functions [41].

Most of the Mg is found in the WH structure. A small amount of Mg enters the HAP structure as well as the organic part of the bone matrix. It is one of the most important divalent ions associated with biological calcium phosphates, affecting all stages of skeletal formation, and therefore the maintenance of homeostasis of this element is essential for the maintenance of good bone tissue condition. Magnesium plays a key role in bone and mineral homeostasis since it affects the formation and secretion of hormones that regulate skeletal homeostasis and bone cell function, and influences hydroxyapatite crystal formation and growth [42].

Several direct and indirect mechanisms contribute to the effects of low Mg on bone density. Magnesium deficiency contributes to osteoporosis directly by acting on crystal formation and bone cells and indirectly by impacting the secretion and the activity of parathyroid hormone and by promoting low-grade inflammation. Magnesemia also promotes inflammation and a relation exists between inflammation and bone loss [43].

In humans, Mg deficiency contributes to osteoporosis and can rapidly lead to hypomagnesemia, which is in part buffered through the mobilization of surface Mg from the bone. Low serum Mg is a co-contributing factor to osteopenia in adults with sickle cell anemia [44].

These results are in keeping with some data showing that elevated Mg might have harmful effects on osseous metabolism and parathyroid gland function, leading to mineralization defects. Indeed, high bone Mg inhibits the formation of hydroxyapatite crystals by competing with calcium and by binding to pyrophosphate forming an insoluble salt, not degraded by the enzymes. These events contribute also to osteomalacic renal osteodystrophy and adynamic bone disease. In patients with chronic renal failure or individuals undergoing dialysis, serum Mg concentrations are frequently elevated and correlate with mineralization defects [45].

Overall, an optimal range of Mg concentrations might be required to ensure bone homeostasis. More studies are required *in vitro* and *in vivo* about the effects of high Mg concentrations on bone metabolism and structure not only to provide correct nutritional guidelines but also because of the use of Mg as high-demand orthopedic implant material [46].

1.3.2 Biological role of manganese in the human body

According to data in the literature, bone represents one of the main deposition tissues of Mn (containing about 43% of total body Mn). Mn exists in different oxidation states, of which Mn^{2+} and Mn^{3+} are the most important from a biological point of view. Moreover, it is a cofactor for many enzymes, including manganese superoxide dismutase, arginase, and pyruvate carboxylase. Through the action of these enzymes, manganese is involved in amino acid, cholesterol, glucose, and carbohydrate metabolism; reactive oxygen species scavenging; bone formation; reproduction; and immune response. It is especially important for normal prenatal and neonatal development [47].

It has been shown to stimulate the synthesis of chondroitin sulfate, an important constituent of the cartilage and connective tissue. There is limited evidence that some disorders or diseases in humans such as amyotrophic lateral sclerosis, acromegaly, catabolic disease, and epilepsy may be associated with an imbalance in tissue levels of Mn. Manganese is an essential element that is required for many biological processes including bone health, macronutrient metabolism, and defense against ROS [48]. The beneficial effects of Mn are due to the incorporation of the metal into metalloproteins. A few well known Mn metalloproteins are arginase (the rate-limiting enzyme in urea synthesis), acetyl-CoA carboxylase (critical catalyst for endogenous fatty acid synthesis), phosphoenolpyruvate decarboxylase, and pyruvate carboxylase (gluconeogenesis), Mn superoxide dismutase (mitochondrial antioxidant), glutamine synthetase (critical for brain ammonia metabolism), and glycosyltransferases (bone health). Tissue contents in mammals are in the range of 0.3–2.9 μg Mn/g wet tissue weight, making Mn one of the most common metals in tissues [49].

1.4 Magnesium whitlockite

1.4.1 Significance in humans

In recent years, advances in the development of synthetic magnesium whitlockite $(Ca_{18}Mg_2(HPO_4)_2(PO_4)_{12})$ have been accompanied by claims that it is the second most abundant inorganic constituent of bone, occupying as much as 20–35 wt% of the inorganic fraction. It is found at many sites in the human body but is particularly concentrated in calcified tissues, such as embryonic and adult bone, as well as in aortic media, where it may be involved in arteriosclerosis [50]. It has also been revealed that magnesium whitlockite appears in abnormal calcification such as dental calculi, kidney stones, or dystrophic calcifications of tuberculous origin. The highest concentrations of whitlockite are found in the weight-bearing area of the femoral head, whereas traces of whitlockite have also been transpired in tuberculous lesions, urinary calculi, and prostatic deposits [51].

From the chemical standpoint, magnesium whitlockite is stable under acidic pH, soluble in physiological solvents, and has a negative surface charge. Acidic conditions promote the integration of the organic matrix into bone tissue and accelerate bone mineralization [52]. During bone maturation, whitlockite undergoes a dynamic phase transition to HAP, a major inorganic component of human solid tissue that provides bone strength and adequate mechanical properties. Synthetic whitlockite (Mg-WH: $Ca_{18}Mg_2(HPO_4)_2(PO_4)_{12}$) nanoparticles can recapitulate early-stage of bone regeneration through stimulating osteogenic differentiation, prohibiting osteoclastic activity, and transforming into mechanically enhanced hydroxyapatite (HAP)-neo bone tissues by the continuous supply of PO_4^{3-} and Mg^{2+} under physiological conditions [53]. These phenomena are essential in the processes of bone formation. Therefore, WH implants can replicate the early stages of bone tissue recovery and accelerate healing processes by ensuring better integration of the implant into natural bone tissue [50].

1.4.2 Crystal structure

For a long time, the name „whitlockite" was used as an alternative name for β-TCP due to the structural resemblance and identical XRD patterns of both of these compounds. Even though the structure of WH is similar to that of β-TCP, these substances cannot be considered isostructural. The structure of whitlockite differs from β-TCP due to the presence of the HPO_4^{2-} group and the fact that some Ca^{2+} ions are replaced by Mg^{2+} ions [52].

Whitlockite is characterized by a rhombohedral structure with *R3c* spatial group and lattice parameters a = b = 10,350 (5) Å, c = 37,085 (12) Å. The crystalline structure of whitlockite is shown in Figure 5 (Fig. 5a, b). The structure of this material periodically repeats two atomic columns: A: Mg - HPO_4 and B: Ca(1) - PO_4 - PO_4 - Ca(2) - Ca(3) (Fig. 5d).

Column A contains MgO_6 octahedral and HPO_4^{2-} groups and column B contains three CaO_8 polyhedral separated by two PO_4 tetrahedrons. Each A-column is surrounded by six B-columns,

while each B-column is surrounded by two A-columns on opposite sides and four B-columns (Figure 5b). The Ca(1) ions belonging to the B chain are directly attached to the three PO_4^{3-} groups (Fig. 5e). One of these PO_4^{3-} groups are directly bound to Mg. The Mg^{2+} ion is surrounded by six PO_4^{3-} groups (Fig. 5h). The Ca(2) position is surrounded by HPO_4^{2-} and three PO_4^{3-} groups (Fig. 2f), and the Ca(3) position is surrounded by three PO_4^{3-} groups (Fig. 5g). In total, 5 cationic positions in the WH structure potential may be occupied by replacement ions [51].

The coordination number of Ca(5) position and O atoms are higher than in other Ca positions, and in the case of the Ca(4) position this number is the lowest, therefore Mg^{2+} ions in WH structure tend to occupy Ca(5) crystallographic positions and Ca(4) crystallographic positions are more likely to become vacancies. The positions of Ca(4) and Ca(5) belong to the A chain. Due to the vacancies in the Ca(4) position, this chain has a half-density lower than that of the B chain [53].
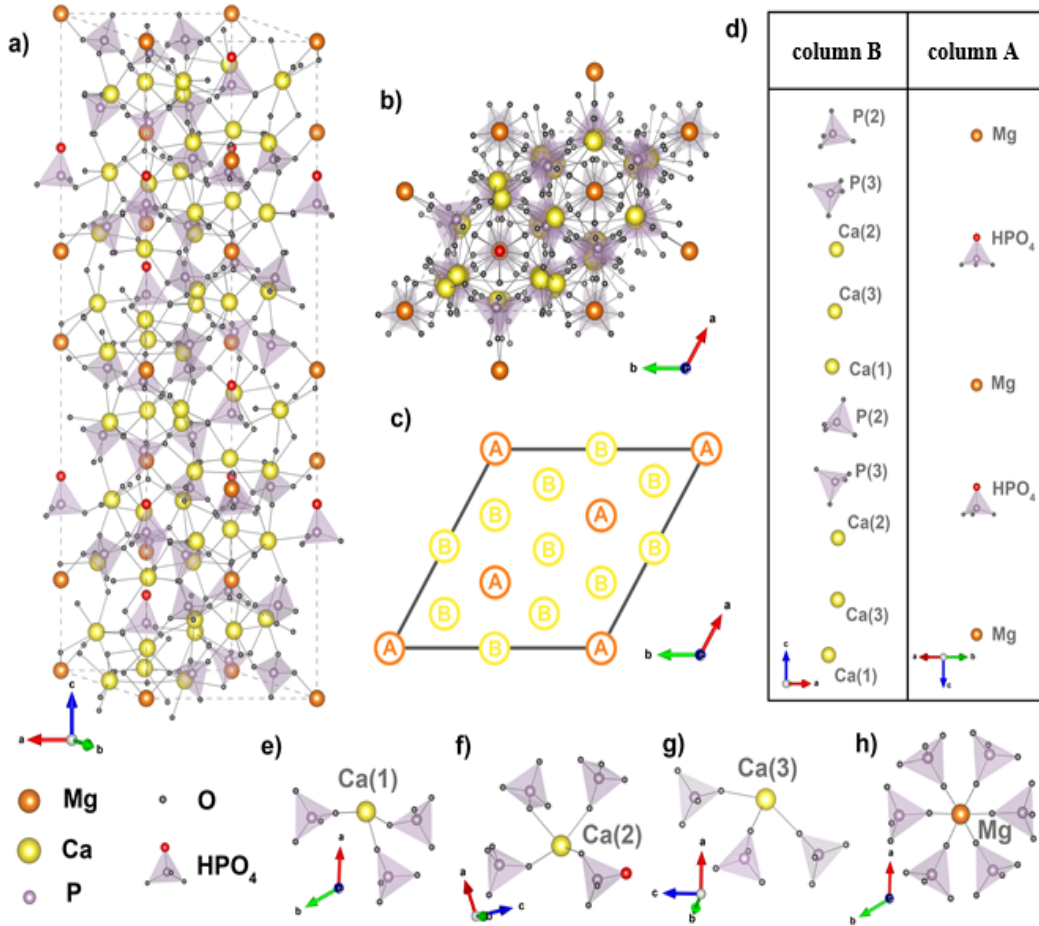

Fig. 5. WH crystal structure: a–b) Scheme of elementary cell; c) Layout of columns A and B; d) Scheme of columns A and B; e–h) Cationic crystallographic positions surrounded by phosphate groups [54].

17

1.5 Whitlockite synthesis methods

Being the second most abundant bio-mineral in living bone, whitlockite is considered to be a quite promising material for use in regenerative medicine purposes. However, the synthesis of pure phase whitlockite remains a challenge due to its poor thermal stability, high sensitivity to synthesis conditions, and a large amount of possible intermediate phases [51].

One of the first methods to obtain synthetic whitlockite was a hydrothermal reaction by heating an amorphous phosphate gel in a stainless-steel bomb. The gel was precipitated from a slightly acidic solution, containing $NH_4H_2PO_4$, $Ca(NO_3)_2$, and $Mg(NO_3)_2$, by rapidly adding concentrated ammonia. The resulting precipitate, a gel, was separated by centrifuging, then spread on filter paper and dried in air at 110 °C. The crushed dried gel half-filled a gold tube, 6 mm in diameter and 10 cm long, with one end welded. The remaining space was filled with distilled water and the top crimped shut. The optimum conditions for the synthesis of coarse crystalline Mg-whitlockite are 300 °C, and 1.5 kbar for 2 weeks [55].

It has been also reported that WH powders can be synthesized by precipitation method using $Ca(OH)_2$, $Mg(OH)_2$, and H_3PO_4 as starting materials. After mixing the $Ca(OH)_2$ and $Mg(OH)_2$ solutions, the required amount of H_3PO_4 was added dropwise with vigorous stirring. A constant temperature of 80 °C was maintained throughout the synthesis. After 24 hours the resulting precipitate was filtered and dried. In other literature sources, this method has been slightly modified by varying the temperature and duration of synthesis [56].

WH can be synthesized using the solvate thermal synthesis method. A three-solvent system was first formed for this purpose: a certain amount of oleic acid and ethanol was stirred for 10 min., then the required amount of 2.5 M NaOH solution was slowly added dropwise to the mixture. The required amount of $CaCl_2$, $MgCl_2$, and Na_2HPO_4 was then added to the resulting solution. Deionized water was then added to the mixture and this was stirred for an additional 30 minutes. Finally, the solution was placed in a stainless steel autoclave and heated at 200 °C for 12 h. The reaction products were washed with ethanol and dried under a vacuum at 60 °C for 12 hours. WH crystals with different morphology were obtained in this way [57].

WH can also be obtained using DCPD as starting material. For synthesis by hydrothermal method, WH samples were obtained by placing a volume of DCPD in a 1.5 mM $MgCl_2$ solution. The powdered solutions were poured into screw-on bottles, screwed on, and placed in a drying oven. The hydrothermal transformation of DCPD crystals into single-phase whitlockite was observed over the period of 1 to 21 d and at 37 °C, 70 °C, and 115 °C unstirred biologically relevant solutions developed for the work. Phase-pure WH crystals with a size of about 200 nm were obtained in this way [9].

WH can also be grown on the surface of other calcium phosphates, such as β-TCP. For this purpose, ceramics (tablet diameter 10 mm) were first formed from β-TCP powder. The whitlockite coating was grown on the surface of the formed β-TCP tablets by the hydrothermal method. The PTFE liners were sealed in a stainless steel autoclave with 120 ml of saline. The reaction was

carried out at 120 °C for 6 hours up to 4 days. The reaction products were washed with acetone and distilled water and dried at 50 °C overnight [58].

WH can also be synthesized in the form of hollow microspheres. WH microspheres were synthesized using a microwave reactor using $CaCl_2$, $MgCl_2 \cdot 6H_2O$, and 1,6-bisphosphate trisodium salt (FBP) as starting materials. An amount of starting material was dissolved in distilled water at room temperature to maintain a constant pH of 9 by slowly adding 1 M aqueous NaOH to the solution. The resulting solution was poured into a Teflon reactor vessel, sealed, and placed in a microwave reactor. The reaction was performed at 120-180 °C for 10-60 min. The reaction products were centrifuged, washed with deionized water and ethanol, and dried at 60 °C for 24 h. The best-performing WH microspheres were synthesized at 120 °C for 10 min. In this way, microspheres can also be obtained using adenosine 5-triphosphate disodium instead of FBP. WH microspheres synthesized in both ways were characterized by excellent biocompatibility and promotion of cell adhesion [59].

WH microspheres can also be obtained using a hydrothermal synthesis method. During the synthesis by this method, a certain amount of starting materials ($CaCl_2$, $MgCl_2 \cdot 6H_2O$, FBP) is dissolved in distilled water. During this process, the pH of the solution was kept constant by slowly adding 1 M aqueous NaOH dropwise. The reaction mixture was placed in a stainless steel autoclave and heated at 180 °C for 1 to 24 h. The resulting WH microspheres were centrifuged, washed with deionized water and ethanol, and dried at 60 °C for 24 h. The best-performing WH microspheres were synthesized at 180 °C for 24 h [60].

WH can also be formed as a by-product of HAP synthesis in the presence of Mg^{2+} or other WH-promoting ions in the reaction mixture. This was the case when the bones of cuttlefish (Sepia Officinalis L.) were selected as the starting material for HAP synthesis. Fishbones were first crushed and treated with NaClO solution. After treatment, the bones were placed in a stainless steel autoclave with a volume of 0.6 M aqueous $NH_4H_2PO_4$. The amount of $MgCl_2 \cdot 6H_2O$ added to the reaction mixture was also such that the ratio of metals to phosphorus in the reaction mixture was 10:6. In all samples containing magnesium, the WH impurity phase formed [61].

2. EXPERIMENTAL

2.1 Materials and solutions

The following materials were used for the synthesis of WH:
- Ammonia solution (NH_3 (aq.), 25%, Roth);
- Magnesium acetate tetrahydrate ($Mg(CH_3COO)_2 \cdot 4H_2O$, $\geq$ 99%, Roth);
- Manganese acetate tetrahydrate ($Mn(CH_3COO)_2 \cdot 4H_2O$, $\geq$ 99%, Roth);
- Calcium hydrogen phosphate dihydrate ($CaHPO_4 \cdot 2H_2O$, pure, Eurochemicals);
- 1 M phosphoric acid solution prepared from concentrated phosphoric acid (H_3PO_4, 25%, Roth).

2.2 Equipment

X-ray diffraction (XRD) analysis was performed by using an X-ray diffractometer Rigaku MiniFlex II (X-ray source Cu-Kα, λ = 1.5419 Å, 40 kV, 100 mA). Measurements were performed in the 2θ range of 10–60°, 1°/min. The obtained data was used for phase identification and purity evaluation. For the Rietveld refinement, information was analyzed in the 10–100° 2θ range. The FullProf Suite was used to refine the structure (FullProf Suite software version September-2020).

The synthesized compounds were also examined by Fourier transform infrared spectroscopy (FTIR). A Bruker ALPHA-FTIR spectrometer was used to record the spectra. Spectra were recorded in the 4000-400 cm^{-1} range for 25 scans.

Raman spectra were recorded using inVia Raman (Renishaw, United Kingdom) spectrometer equipped with a thermoelectrically cooled (–70 °C) CCD camera and microscope. Raman spectra were excited with a 325 nm beam from the continuous wave helium-cadmium (He-Cd) gas laser. The laser power at the sample was restricted to 0.2 mW. The 15x/0.32 NA objective was used during the measurements. The high-resolution Raman spectra were observed with 532 nm excitation wavelength, 3000 lines/mm grating, and 20x/0.40 NA objective. The laser power at the sample was 0.5 mW. Parameters of the bands were determined by fitting the experimental spectra with Gaussian-Lorentzian shape components using GRAMS/A1 8.0 Thermo Scientific, USA) software.

A Hitachi SU-70 scanning electron microscope was used to investigate the morphology of the produced compounds (SEM).

The XPS analyses were carried out with a Kratos Axis Supra spectrometer using a monochromatic Al-Kα source (25 mA, 15 kV). XPS can detect all elements except hydrogen and helium, probes the surface of the sample to a depth of 5-7 nanometers, and has detection limits ranging from 0.1 to 0.5 atomic percent depending on the element. The instrument work function was calibrated to give binding energy (BE) of 83.96 eV for the Au 4f7/2 line for metallic gold and the spectrometer dispersion was adjusted to give a BE of 932.62 eV for the Cu 2p3/2 line of metallic copper. The Kratos charge neutralizer system was used on all specimens. Survey scan

analyses were carried out with an analysis area of 300×700 microns and a pass energy of 160 eV. High-resolution analyses were carried out with an analysis area of 300×700 microns and a pass energy of 20 eV. Spectra have been charge corrected to the mainline of the carbon 1s spectrum (adventitious carbon) set to 284.8 eV. Spectra were analyzed using CasaXPS software (version 2.3.23rev1.1R).

Thermal decomposition of synthesized powders was analyzed by thermogravimetric and differential scanning calorimetric (TG-DSC) analysis using Perkin Elmer STA 6000 Simultaneous Thermal Analyzer. A dried sample of about 20 mg was heated from 25 to 900 °C with a heating rate of 10 °C/min in dry flowing air (20 mL/min).

N_2 adsorption and desorption isotherms of the samples were measured at 196 °C using the Brunauer–Emmett–Teller (BET) analyzer TriStar II 3020, Micromeritics. All of the samples were outgassed in an N_2 environment at 100 °C for 2 hours before the gas sorption tests.

To investigate thermal stability, Mg-WH samples were annealed at a temperature range of 400−1300 °C at the 100 °C steps using a laboratory furnace (SNOL 8,2/1100 LSM01).

2.3 Synthesis

2.3.1 Dissolution-precipitation synthesis of Mg-WH under hydrothermal conditions

For the synthesis of Mg-WH, calcium hydrogen phosphate dihydrate ($CaHPO_4 \cdot 2H_2O$, 99.1 %, Eurochemicals) and magnesium acetate tetrahydrate ($Mg(CH_3COO)_2 \cdot 4H_2O$, ≥ 99.5%, Roth) were used as precursors. After weighing the precursors, 50 mL of distilled water and 5.6 mL of 1 M H_3PO_4 solution were added. To achieve a requisite chemical composition of the product, the precursors were mixed corresponding to a Ca-to-Mg molar ratio of 9 and the total concentration of Ca and Mg ions in the reaction mixture was 0.007 M. Then PTFE liner containing starting materials was put on magnetic stirrer without additional pre-heating and the mixture was stirred for 1 h to obtain a clear and homogeneous solution. After the stirring procedure, the pH of the solution was adjusted to 6.4 with a concentrated ammonia solution (NH_4OH, 25%, Roth). After the achievement of the target pH, the PTFE liner was sealed in a stainless steel reactor and placed in a laboratory oven for 3 h at 160 °C. The resulting precipitate was filtered, washed with distilled water, and dried at 60 °C in the oven. The synthesis scheme is represented in Fig. 6**.**
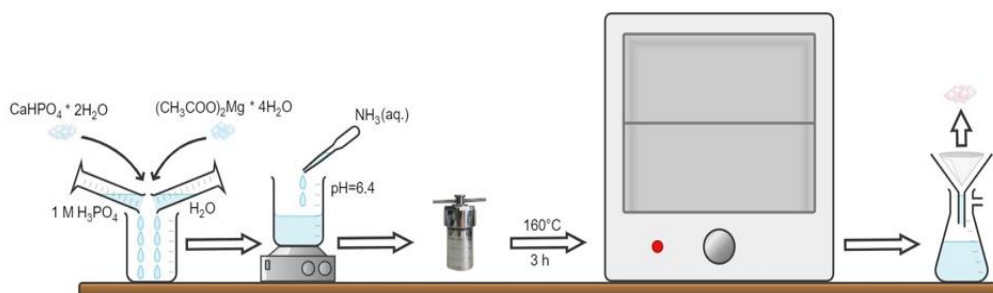

Fig. 6. Mg-WH synthesis scheme.

2.3.2 Dissolution-precipitation synthesis of Mn-WH

For the synthesis of Mn-WH powders, calcium hydrogen phosphate dihydrate $(CaHPO_4 \cdot 2H_2O$, 99.1 %, Eurochemicals) and manganese acetate dihydrate $(Mn(CH_3COO)_2 \cdot 4H_2O$, ≥ 99.5%, Roth) were used as starting materials.

All chemicals were used as received without additional purification. For the synthesis certain amount of $CaHPO_4 \cdot 2H_2O$ and $Mn(CH_3COO)_2 \cdot 4H_2O$ corresponding to a Ca-to-Mn molar ratio of 9 were dissolved in a mixture of 100 mL of distilled water and 13 mL of 1 M phosphoric acid $(H_3PO_4$, 75%, Roth). The temperature of the obtained solution was set to 75 °C, and the mixture was stirred for 1 hour to obtain a clear homogeneous solution. During the stirring procedure, the pH of the solution was precisely measured several times and was approximately 2.7. Next, under constant mixing on a magnetic stirrer, aqueous ammonia solution $(NH_4OH$, 25%, Roth) was added drop by drop to adjust the pH to 5.6. The increase in the pH value of the reaction medium resulted in the instantaneous formation of white precipitates. Afterward, the resulting mixture was poured into a reagent bottle and placed in the shaker incubator (Biosan ES-20/80) for 3 h at 75 °C and a rotating speed of 220 rpm. At the end of the synthesis, the precipitates were vacuum-filtered, washed with distilled water, and dried at 60 °C in an oven overnight. A schematic representation of the synthesis procedure is shown in Fig. 7.
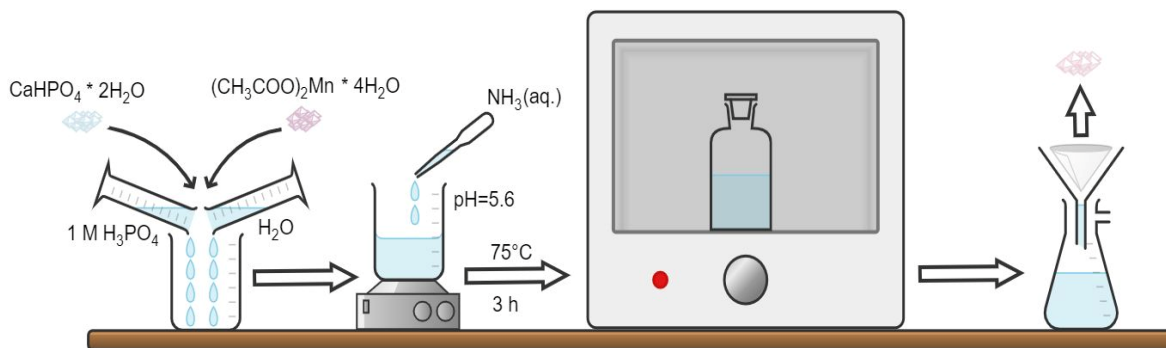

Fig. 7. Mn-WH synthesis scheme.

3. RESULTS AND DISCUSSION

3.1 Mg-whitlockite

CaP have found a huge application in regenerative medicine in the form of ceramics, the manufacturing of which is usually associated with the high-temperature heat treatment of powders. This process of producing ceramics is not suitable for thermally unstable substances. Therefore, the powder was heated in the temperature range of 400−1300 °C to evaluate the thermal stability of the produced Mg-WH compounds. The XRD patterns of Mg-WH powders annealed at different temperatures are represented in Fig. 8.
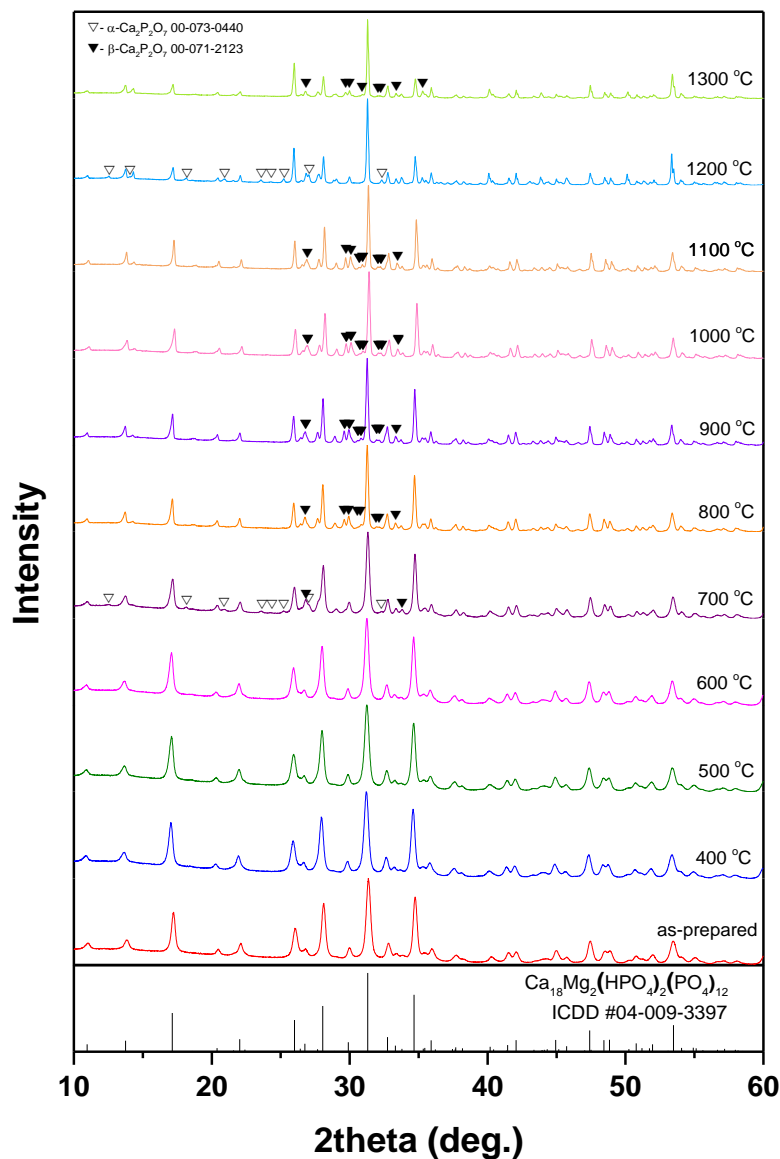
Fig. 8. XRD patterns of pristine Mg-WH powders annealed at different temperatures.

No visible changes and newly aroused diffraction peaks were noticed in the XRD pattern after annealing at 400 °C. However, after the heat treatment at higher temperatures, the appearance of additional peaks was observed. The formation process of α-$Ca_2P_2O_7$ and β-$Ca_2P_2O_7$ starts at around 700 °C. The XRD patterns of the powders annealed at 800 °C, 900 °C, 1000 °C, and 1100 °C are dominated by the reflections of β-$Ca_3(PO_4)$ and secondary β-$Ca_2P_2O_7$ phase. Further increase in annealing temperature resulted in a gradual phase transformation of β-$Ca_2P_2O_7$ to α-$Ca_2P_2O_7$ at 1200 °C. After reaching 1300 °C the complete transformation of α-$Ca_2P_2O_7$ to β-$Ca_2P_2O_7$ occurs.

Therefore, it has been revealed that synthesized Mg-WH powders are thermally unstable and decomposed upon heat treatment with the formation of β-$Ca_3(PO_4)$, α-$Ca_2P_2O_7$, and β-$Ca_2P_2O_7$ phases. It has also been observed that increasing the annealing temperature increased crystallinity, as evidenced by the gradual sharpness of the diffraction peaks.

As XRD patterns of WH and β-TCP are difficult to distinguish, the use of vibrational spectroscopy is crucial for the comprehensive characterization of WH powders and confirmation of the presence of various functional groups. Chemical functional group frequency analysis is used in infrared and Raman spectroscopies to detect the molecular components of substances. These approaches are sensitive to the material's crystallographic site symmetry, allowing differentiation between crystallographically identical structures. FTIR spectra of synthesized Mg-WH powders in the representative spectral range of 1400−400 cm^{-1} are demonstrated in Fig. 9.
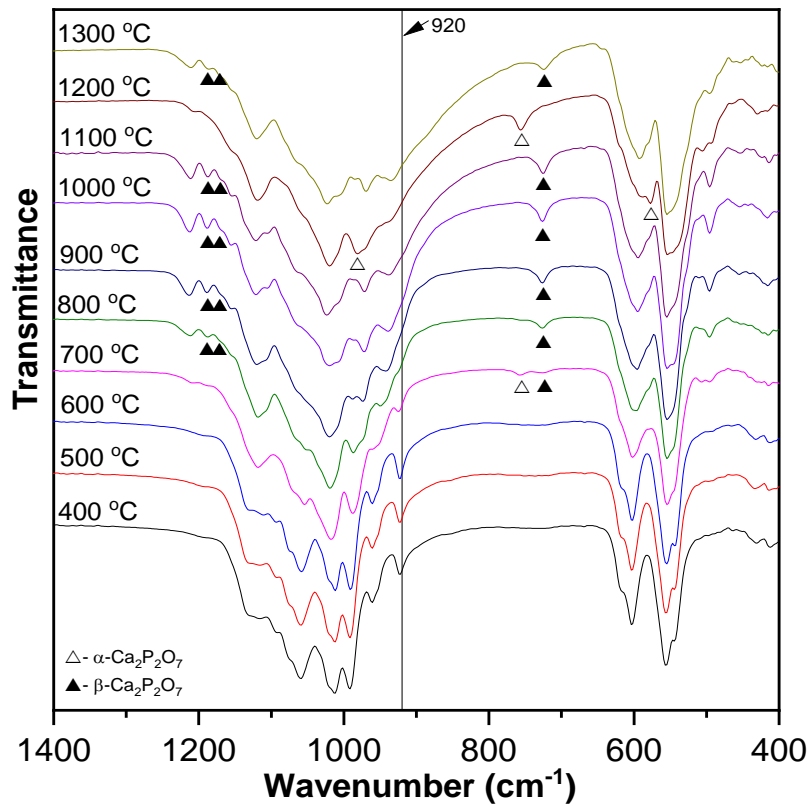

Fig. 9. FTIR spectra of Mg-WH powders annealed at different temperatures.

The most intense absorption bands correspond to the vibrations of phosphate functional groups. The absorption bands in the range from approximately 1200 to 930 cm^{-1} correspond to the phosphate v_3 and v_1 stretching modes. The bands in the 640−500 cm^{-1} region and at 436 cm^{-1} are also characteristic of phosphate groups and ascribed to the v_4 and v_2 bending modes, respectively. It should be noted that the absorption band at 920 cm^{-1}, corresponding to HPO_4^{2-}, after annealing at 700 °C became less intense. For the identification of WH, attention must be paid to the absorption band located at 920 cm^{-1}, indicative of HPO_4^{2-} and suggesting WH phase.

The disappearance of the indicative band has been observed at an annealing temperature of 800 °C which refers to phase transformation from WH to the β-$Ca_3(PO_4)$ and calcium pyrophosphate phase. A possible explanation for this change could be found in the increase in the degree of crystallinity after the heat treatment, and thus the results obtained showed the thermally unstable nature of the synthesized materials.

Raman spectra of synthesized Mg-WH samples annealed at different temperatures are depicted in Fig. 10.
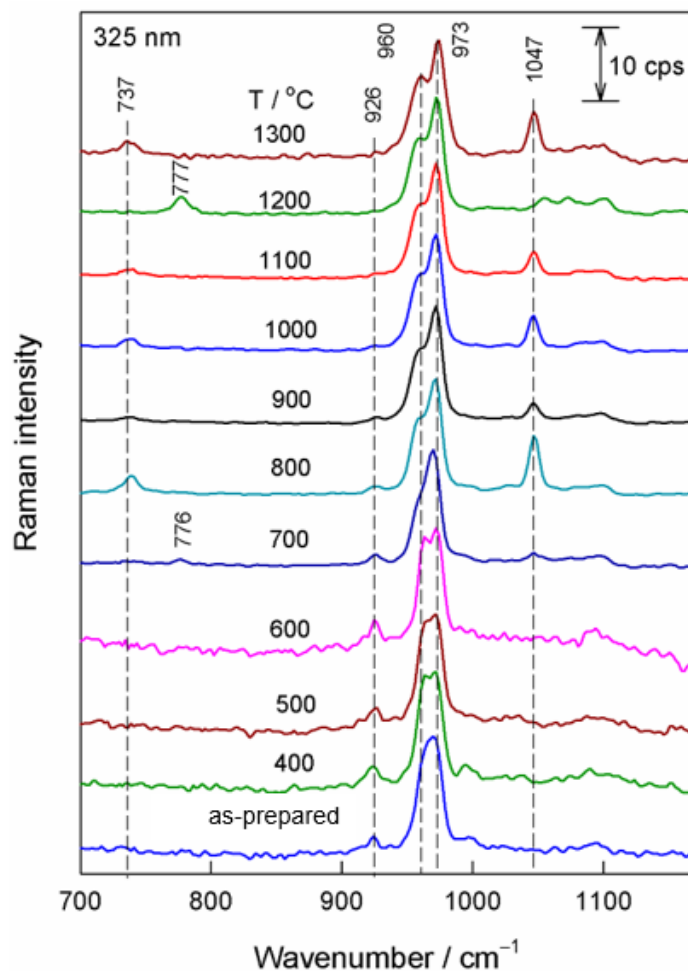

Fig. 10. Raman spectra of whitlockite-type compounds annealed at different temperatures.

Characteristic bands can be observed in the ranges of approximately 990−1125 cm^{-1} (v_3). The most intense band centered at 973 cm^{-1} is ascribed to the v_1 symmetric stretching vibrational mode. All these bands are also present in the Raman spectra of β-TCP and associated with internal vibrations of PO_4^{3-} ions.

The remarkable feature of the obtained Raman spectra of as-prepared Mg-WH powder is the visible band at 926 cm^{-1}, which is the characteristic spectral marker for HPO_4^{2-} which corresponds to the WH structure of the synthesized compound. However, it can be clearly seen that with each increase in annealing temperature the band became less distinct and at the annealing temperature of 1300 °C it almost disappears. Therefore, it can be concluded that vibrational spectroscopy supported the results of FTIR analysis and demonstrated that obtained Mg-WH powders are thermally unstable.

SEM was used to study the morphology of the synthesized Mg-WH powder. Fig. 11 represents the most distinct micrographs of the surface morphology of the as-prepared Mg-WH samples and annealed at different temperatures of 400 °C, 600 °C and 800 °C.
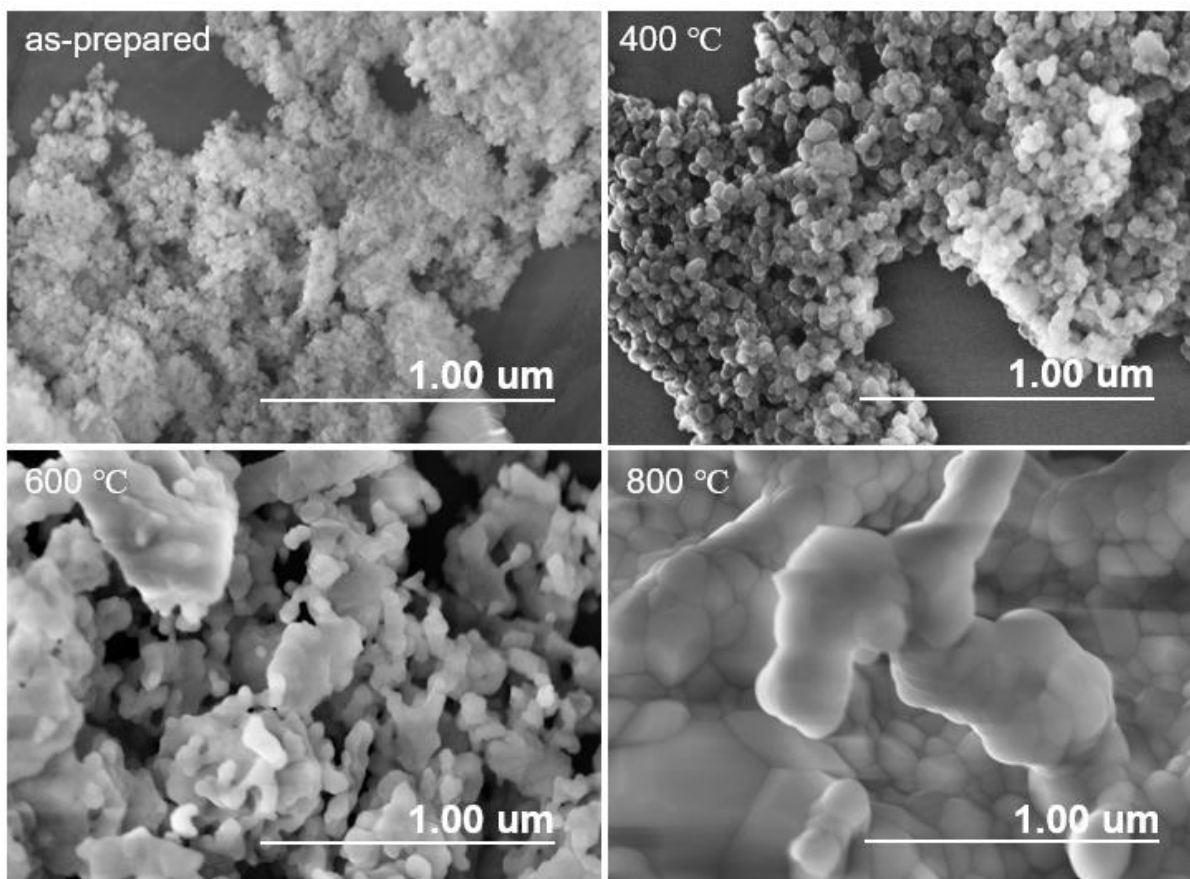

Fig. 11. SEM micrographs of Mg-WH powders synthesized with a Ca-to-Mg ratio of 9.

It has been observed, that as-prepared powder produced is found to be generally homogenous and agglomerated. With the increase in annealing temperature, the micrographs show randomly

distributed and non-uniform clusters. It has been observed that these clusters are a function of annealing temperature, the cluster size increases as the temperature increases, and the increases in cluster size are attributed to the fact that as the temperature increases more particles agglomerated and form a larger cluster.

To investigate the surface area of Mg-WH samples, BET analysis was performed (Fig. 12).
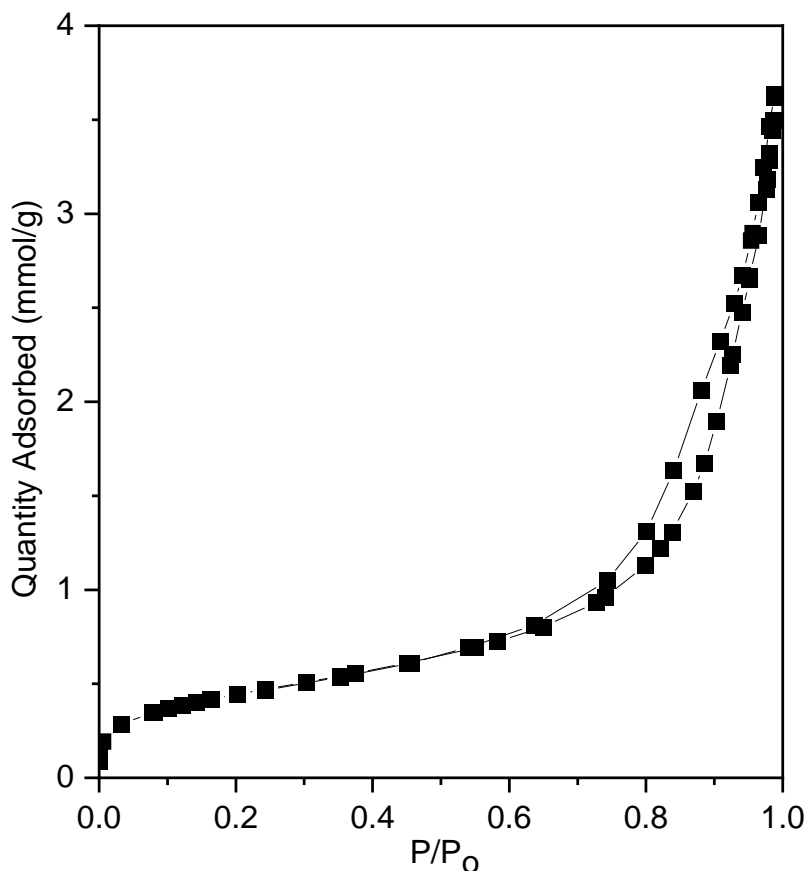

Fig. 12. Adsorption-desorption isotherm graph of Mg-WH powder.

The N_2 adsorption-desorption isotherm of both samples can be classified as type IV with a hysteresis loop type H3. Type IV isotherm indicates that mesopores are dominant in the samples. The type H3 loop is usually observed with aggregates of plate-like particles which give rise to slit-shape pores. This data correlates well with SEM micrographs of the samples as well as pore size distribution results.

The external surface area (S_{ext}), which is corresponding to the mesopore surface area, was determined to be 38.35 m^2/g, and the specific surface area calculated by the BET method (S_{BET}) was found to be 36.65 m^2/g. The total volume of pores (V_{tot}) was found to be 0.12 cm^3/g. S_{ext} and S_{BET} for the 0.12 M sample were determined to be 38.34 and 36.65 m^2/g respectively, and V_{tot} was 0.12 cm^3/g. All of these parameters were found to be bigger in the sample obtained in a larger total metal ion concentration. Micropore volume (V_{μ}) in both samples is <0.01 cm^3/g and confirms that materials are meso- and macroporous.

27

3.2 Mn-whitlockite

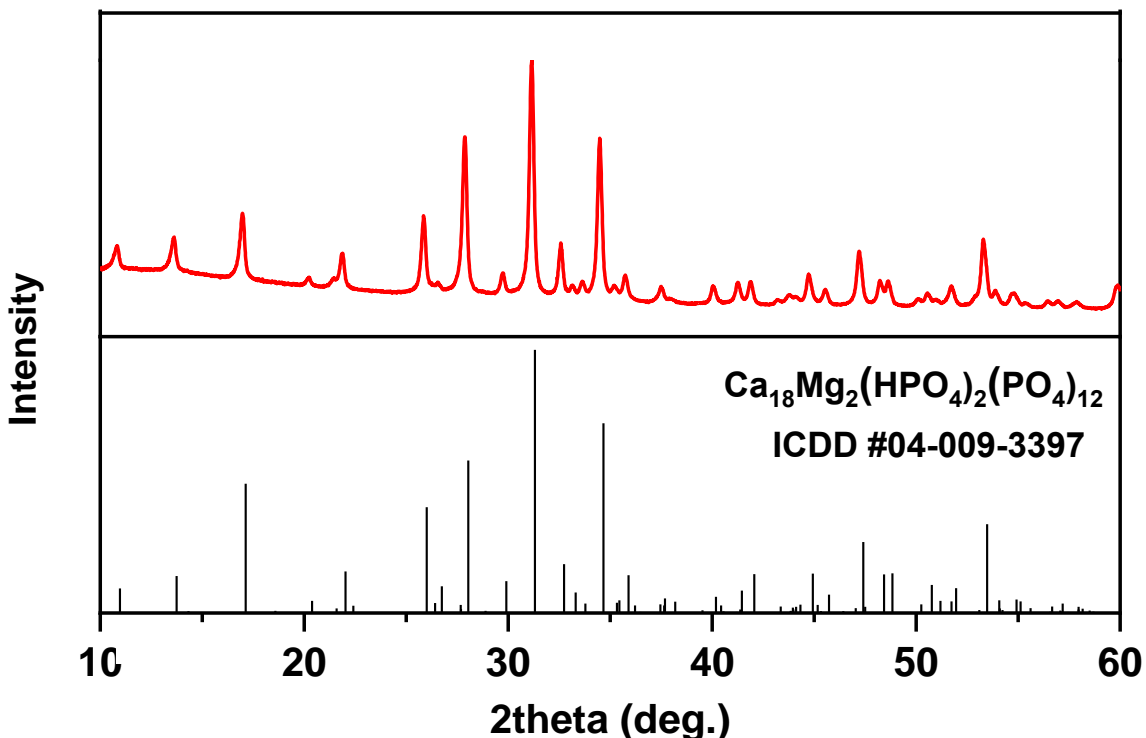The XRD pattern of the synthesized Mn-WH powder with Ca-to-Mn ratio of 9 is represented in Fig. 13.

Fig. 13. XRD pattern of Mn-WH powder.

As seen, all X-ray reflection peaks correspond to the WH crystal phase and peak positions match well with those of Mg-WH (ICDD #04-009-3397). The absence of reflections related to phases other than WH indicates high phase purity of the synthesized powders.

In addition to XRD analysis, Rietveld refinement was performed on the synthesized Mn-WH (Fig. 14). The polycrystalline Mn-WH material was confirmed to have a rhombohedral structure with unit-cell parameters (a = b = 10.36 (2) Å, c = 37.09 (5) Å, $\alpha = \beta = 90°$; and c = 120° in the hexagonal setting (space group R$3c$, Z = 21).

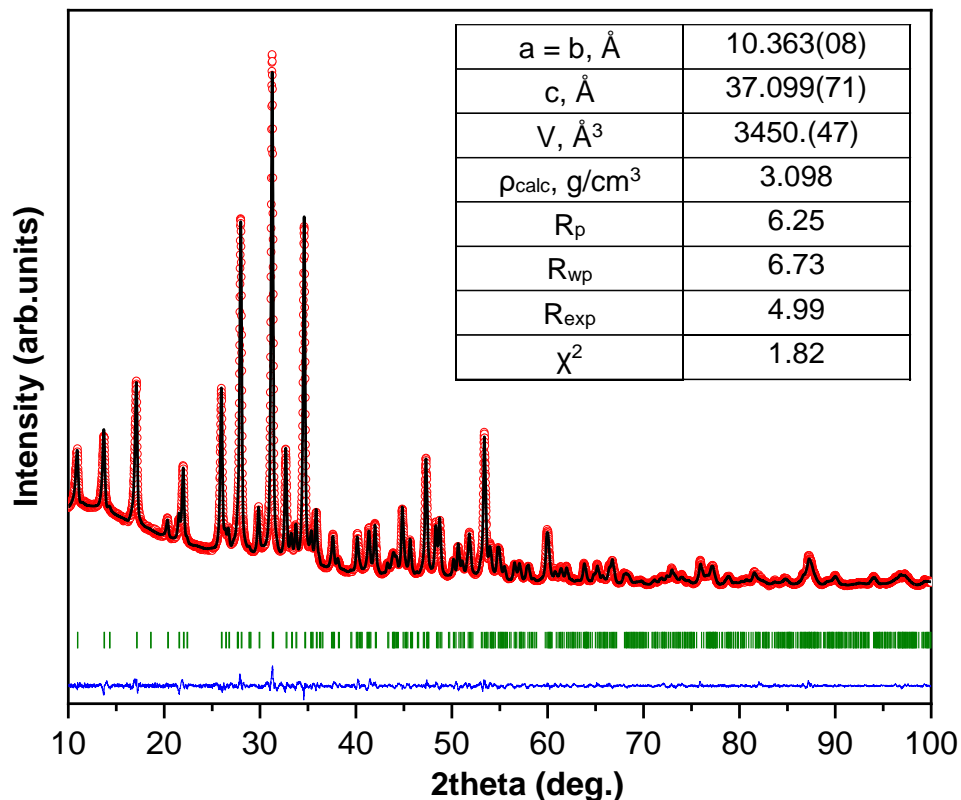| a = b, Å	10.363(08)
c, Å	37.099(71)
V, Å^3	3450.(47)
ρ_{calc}, g/cm^3	3.098
R_p	6.25
R_{wp}	6.73
R_{exp}	4.99
χ^2	1.82

Fig. 14. Rietveld refinement of Mn-WH powder.

As previously mentioned, it is hard to distinguish the XRD patterns of WH and β-TCP; therefore, the use of vibrational spectroscopy is crucial for the full characterization of WH powders and confirmation of the presence of distinct functional groups. The FTIR spectrum of Mn-WH (Fig. 15) shows characteristic bands of the phosphate group (PO_4^{3-}).
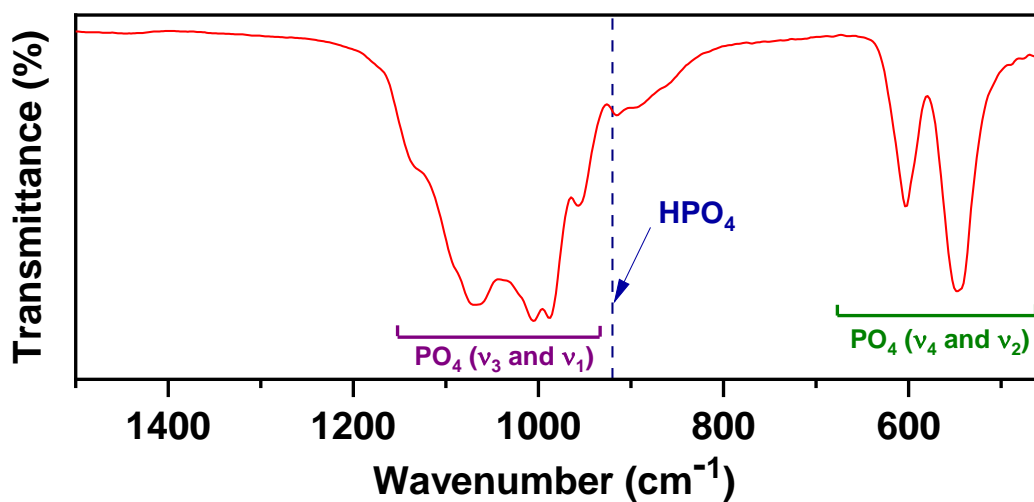

Fig. 15. FTIR spectrum of Mn-WH powder.

The absorption bands between 1200 and 900 cm⁻¹ correspond to the triple degenerated asymmetric stretching mode v_3, and the symmetric stretching mode v_1 of the P−O bonds, while bands between 630 and 450 cm⁻¹ are due to the triple degenerated bending mode v_4 of the O−P−O of PO_4^{3-} group. The distinctive peak observed at 920 cm⁻¹ is indicative of HPO_4^{2-} and suggests the WH phase. Therefore, the FTIR spectrum agrees with the literature data and confirms the WH structure of the synthesized Mn-WH powder.

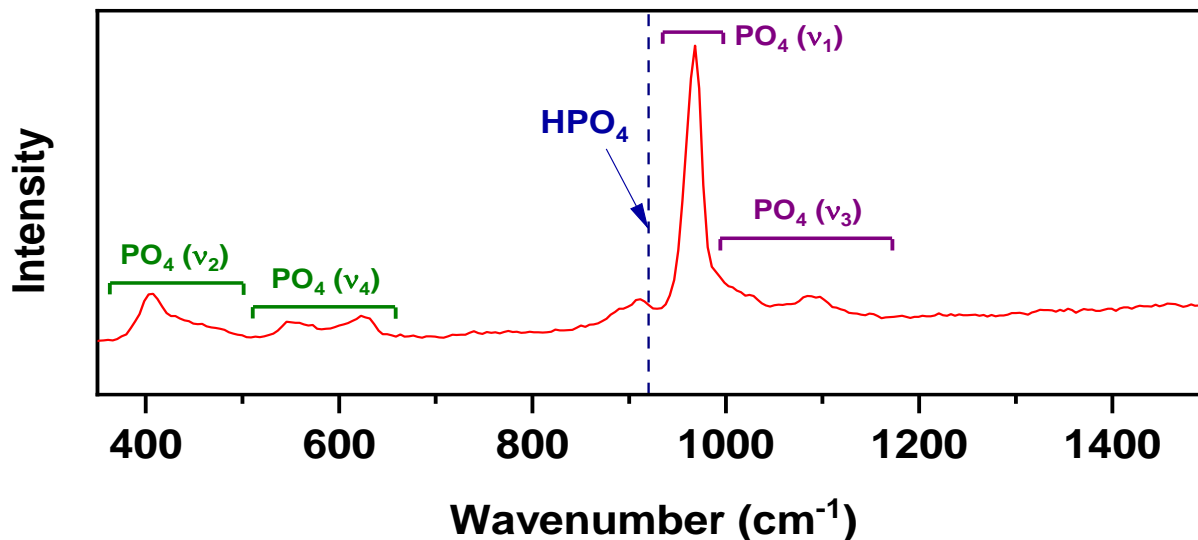The room-temperature Raman spectra of the synthesized Mn-WH powder are shown in Fig. 16.

Fig. 16. Raman spectrum of Mn-WH powder.

Characteristic vibrations of the PO_4^{3-} group appear in the region of 360 – 500 cm⁻¹ and 500 – 720 cm⁻¹. These bands were attributed to the v_2 (PO_4^{3-}) and v_4 (PO_4^{3-}) modes, respectively. In the region of 1200 to 930 cm⁻¹, 2 peaks appear corresponding to the phosphate v_3 and v_1 stretching modes. It can be also observed, that the indicative peak of HPO_4^{2-} appears at 920 cm⁻¹ which is verified by obtained FTIR results and agreed with many previous data in literature.

The low-resolution XPS survey spectrum for the Mn-WH particles can be seen in Fig. 17.
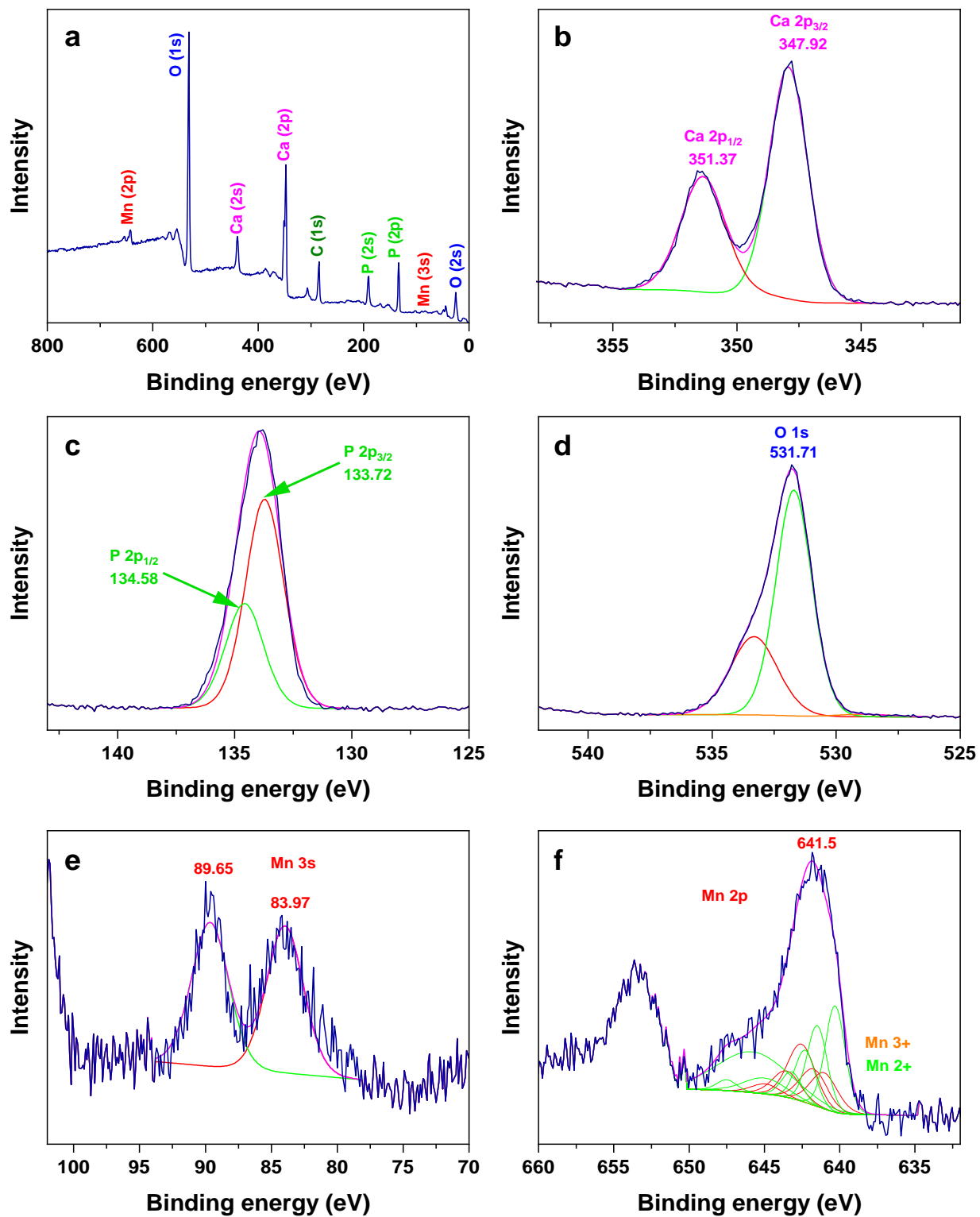

Fig. 17. XPS spectra of Mn-WH powder.

Besides the expected Ca, P, O, and Mn, samples contained a certain amount of C ($1s$). Carbon impurity had an atomic percentage of ~23 %. The C $1s$ or ''adventitious carbon" peak is used as a reference in XPS analysis, and the BE calibration was performed by setting this peak at 285.0 eV for sample charging correction (Fig. 17a). However, a small carbonate-type peak was observed at 289.4 eV, possibly resulting from CO_2 in the air during sample preparation.

High-resolution C $1s$, Ca $2p$, P $2p$, O $1s$, and Mn $2p$ Mn LMM XPS spectra were collected to further reveal the chemical nature of the elements (Fig. 17a). Curve fitting of p core level lines was performed maintaining 3/2 and 1/2 peak area ratio to 2:1. The typical and well-distinguished pairs from spin-orbit spitting, Ca $2p_{3/2}$ and Ca $2p_{1/2}$, were observed in all samples at around 347.92 eV and 351.37 eV (Fig. 17b), respectively, in accordance with the observed elsewhere for calcium compounds. Due to similar phosphorous chemical shifts of PO_4^{3-} and HPO_4^{2-} ions, adequate spectra fit was achieved using two P $2p_{3/2}$ and P $2p_{1/2}$ components at respective BE of 133.72 eV and 134.58 eV (Fig. 17c). P $2p$ phosphate peak energies were similar to their reported value. Fig. 4c shows the O $1s$ high-resolution XPS spectrum with the maximum binding energy of 531.71 eV.

Fig. 17f represents the Mn $2p$ photoelectron lines, in which a doublet peak is observed due to typical Mn $2p_{1/2}$ and Mn $2p_{3/2}$ spin-orbit splitting with the maximum binding energy of 641.5 eV. It was also observed that Mn $3s$ spectra consisted of two symmetric peaks located at 89.65 (Mn $3s_{1/2}$) and 83.97 eV (Mn $3s_{3/2}$). The identification of the different species contributing to the Mn $2p$ XPS spectra is difficult as this element has six stable oxidation states, some of them showing significant multiplet splitting and also overlapping binging energy ranges. However, the binding energy values obtained are in the range of different Mn compounds reported in the literature.

Furthermore, the satellite peak observed at a higher binding energy of the Mn $2p_{3/2}$ peak is typical for the Mn^{2+} state, which could indicate the presence of manganese mainly as Mn^{2+} in the WH structure. However, Mn^{3+} has also been observed as a result of the shift of the Mn $2p$ bands to higher binding energy values. Since X-ray photoelectron spectroscopy (XPS) is the technique for measuring elemental composition on the material surface, the presence of Mn^{3+} ions in the Mn-WH structure can be explained as the oxidation of some manganese on the very surface of the WH powder.

The representative SEM micrographs of Mn-WH powders synthesized with a Ca-to-Mn ratio of 9 are demonstrated in Fig. 18.
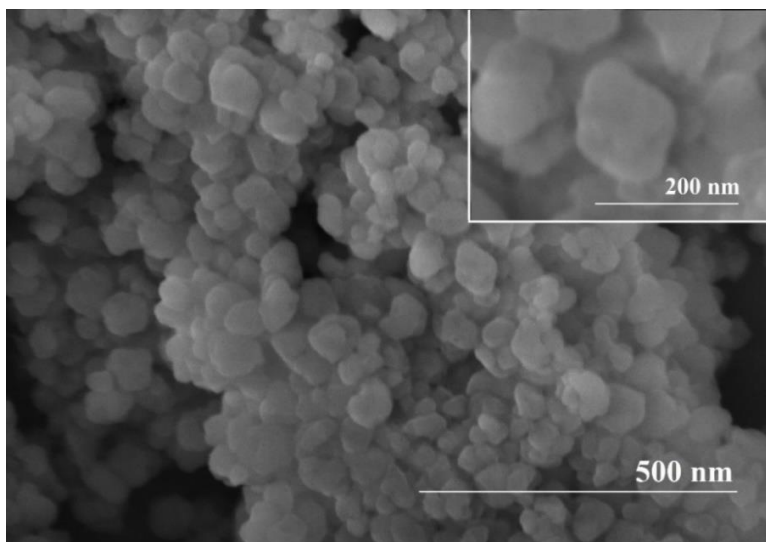
Fig. 18. SEM micrographs of Mn-WH powder.

It is seen that powders synthesized with a Ca-to-Mn ratio of 9 consists of mostly uniform and agglomerated particles. Although synthesized powders are highly agglomerated, a closer look shows that some particles have a very distinctive rhombohedral shape. It can be also seen that there are no crystals with obviously different morphologies, which can be considered as additional indirect evidence of the phase purity of the products.

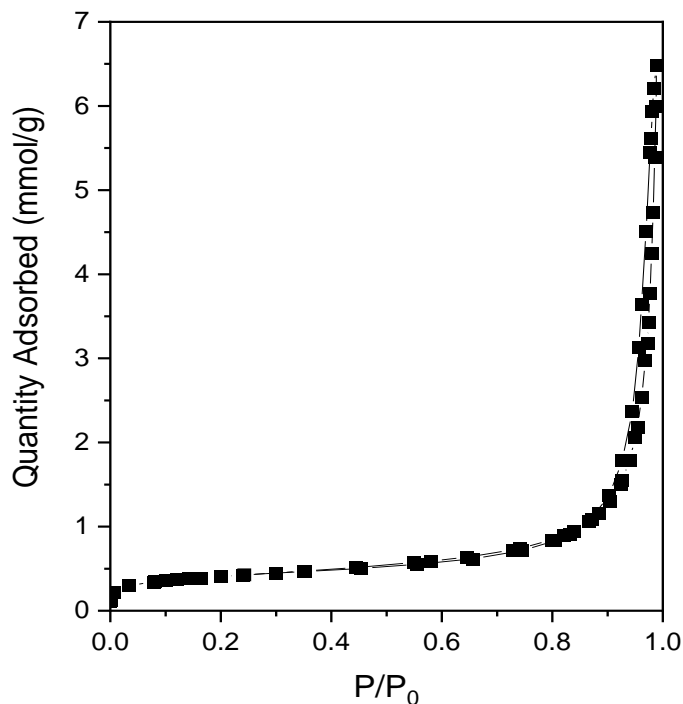The porosity and surface area of Mn-WH samples were measured using BET analysis (Fig. 19 and Fig. 20).

Fig. 19. Adsorption-desorption isotherm graph of Mg-WH powder.

The N_2 adsorption-desorption isotherm of the samples can be classified as type IV with a hysteresis loop type H3. Type IV isotherm indicates that mesopores are dominant in the samples. The type H3 loop is usually observed with aggregates of plate-like particles which give rise to slit-shape pores. This data correlates well with SEM micrographs of the samples as well as pore size distribution results. The pore size distribution curve of the sample obtained shows mesopores with dominant sizes of 4-50 nm and macropores with a range of 55-135 nm.

The powder has a relatively wide distribution of pores ranging from 4 to 135 nm. The external surface area (S_{ext}), which is corresponding to the mesopore surface area, was determined to be 25.49 m^2/g, and the specific surface area calculated by the BET method (S_{BET}) was found to be 32.27 m^2/g. The total volume of pores (V_{tot}) was found to be 0.16 cm^3/g. Micropore volume (V_μ) in both samples is <0.01 cm^3/g and confirms that materials are meso- and macroporous.
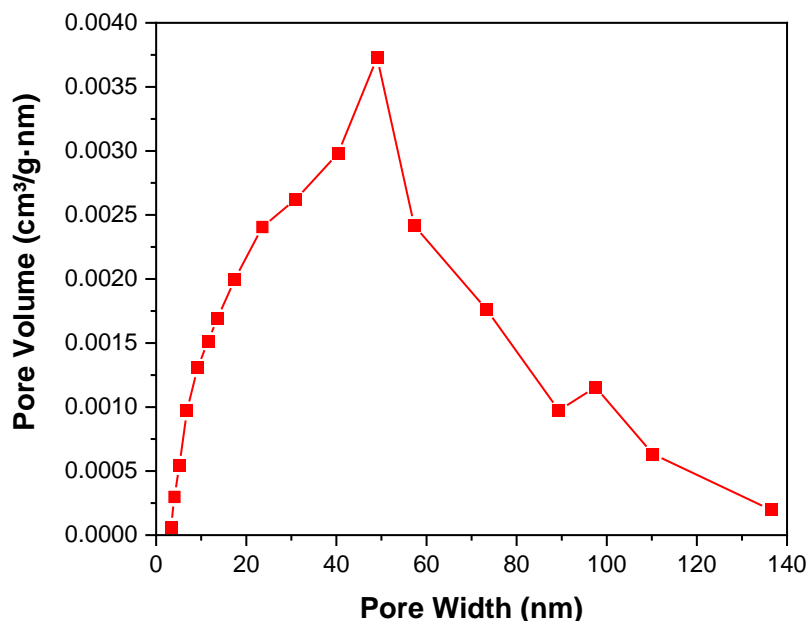

Fig. 20. BJH pore-size distribution curve of Mn-WH powder.

Therefore, the pore diameter observed for all samples confirms that all materials exhibit a pore size in the mesoporous and macroporous range. This is of great relevance for biomedical applications, as pores allow the adsorption of biological agents that could improve the body's response to the material.

The thermal decomposition behavior of as-prepared Mn-WH powder was investigated by simultaneous TG/DTG/DSC (thermogravimetry/differential thermogravimetry/differential scanning calorimetry) measurements to evaluate the thermal stability of the synthesized Mn-WH powder (Fig. 21).
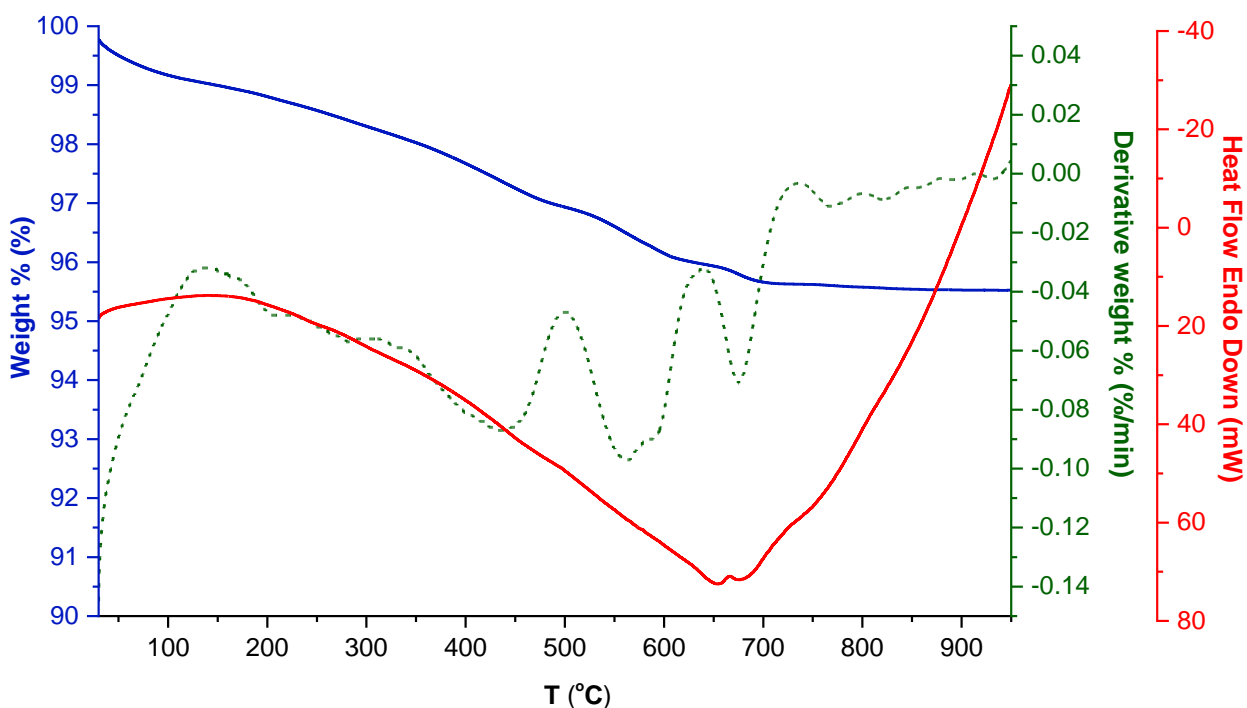
Fig. 21. TG/DTG/DSC curves of as-synthesized Mn-WH powder.

TG/DTG/DSC curves of the as-prepared precipitate are presented in Fig. 20. The total weight loss was calculated to be around 4.5%. The decomposition is attributed to the degradation of Mn-WH structure and the release of crystalline water, leading to the formation of α and β-$Ca_2P_2O_7$. The formation of the P_2O_7 group was also confirmed by FTIR analysis.

The magnetic properties of the synthesized Mn-WH powder have also been investigated. The dependence of magnetic susceptibility vs temperature χ (T) for the Mn-WH sample is presented in Fig. 22.
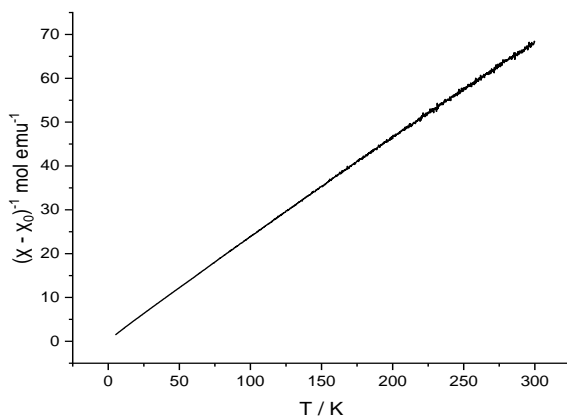

Fig. 22. Inverse magnetic susceptibility, $(\chi - \chi_0)^{-1}$, plotted versus temperature for Mn-WH with a zero-field-cooling mode in an applied field of 100 Oe.

Data were collected upon heating in the temperature range from ~ 5 to 300 K in a fixed applied external magnetic field of 20 kOe after zero-field - cooling (ZFC). All measurements have been repeated a few times during warm-up from 5 up to room temperature. The magnetic susceptibilities always returned to their initial value and the χ (T) curves again were retraced. Fig. 21 shows the inverse proportionality of magnetic susceptibility to the value of the temperature. Temperature increases cause greater thermal vibration of atoms, which interferes with the alignment of magnetic dipoles. The field-dependent magnetization curve of Mn-WH at temperature 5 K is presented in Fig. 23.
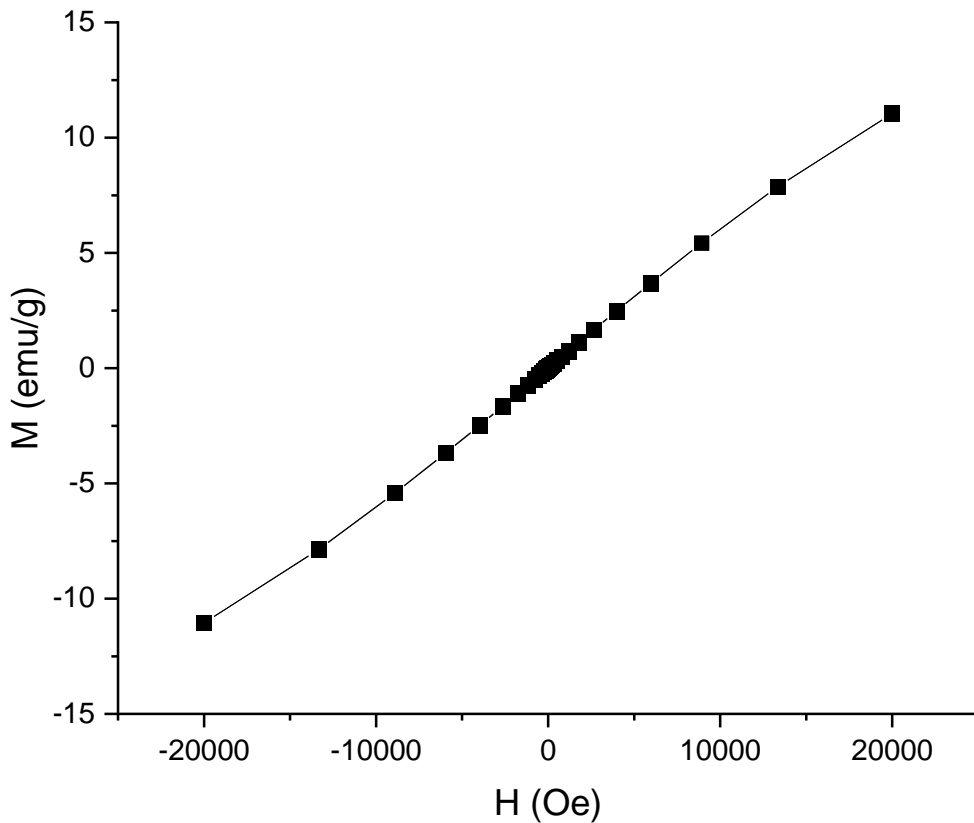

Fig. 23. Field-dependent magnetization curve of Mn-WH at the temperature of 5 K.

It can be seen that there's a linear dependence between magnetization and applied magnetic field at the temperature of 5 K, which is additional direct evidence that synthesized Mn-WH demonstrates paramagnetic properties. The same linear dependence was obtained at room temperature (Fig. 24).
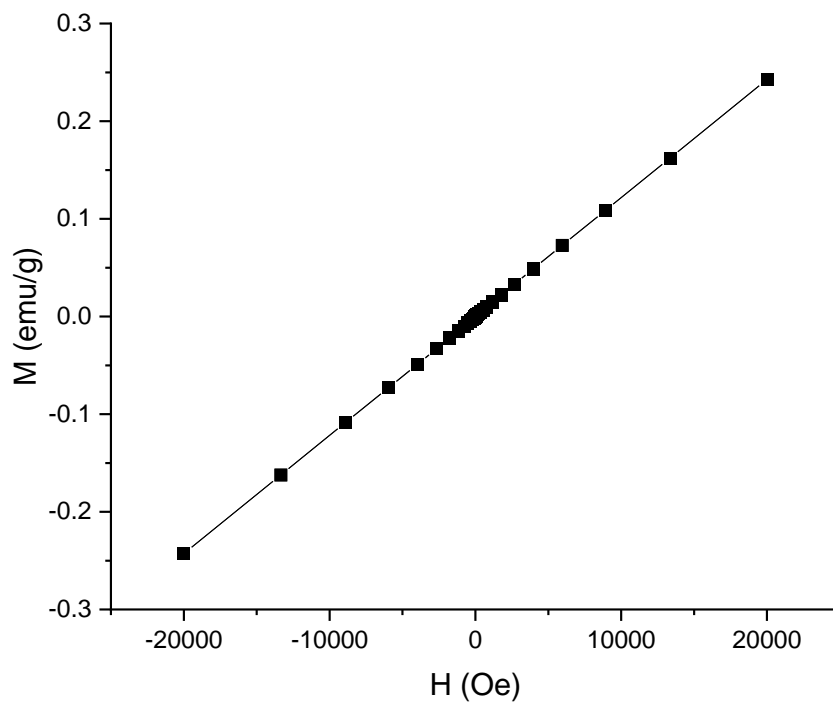
Fig. 24. Field-dependent magnetization curve of Mn-WH at room temperature.

CONCLUSIONS

1. Magnesium whitlockite was successfully synthesized by the dissolution-precipitation process under hydrothermal conditions. Thermal stability studies have demonstrated a thermally unstable nature of the synthesized powder: after the annealing procedure, it decomposes to β-$Ca_3(PO_4)_2$, α- and β-$Ca_2P_2O_7$. It has been revealed, that the decomposition process starts at 700 °C.
2. Low-temperature procedure for the synthesis of manganese whitlockite was developed. To the best of our knowledge, manganese whitlockite was synthesized by the low-temperature synthesis for the first time in this work. XRD analysis and Rietveld refinement confirmed that synthesized material has a rhombohedral structure with the *R3c* space group.
3. Studies on magnetic properties revealed that manganese whitlockite has paramagnetic nature both at 5 K and room temperatures. The paramagnetic susceptibility is inversely proportional to the value of the absolute temperature.

REFERENCES

[1] N. Eliaz, N. Metoki, *Calcium phosphate bioceramics: A review of their history, structure, properties, coating technologies, and biomedical applications*. Materials, **2017**. 10(4): p. 2-6, DOI: https://doi.org/10.3390/ma10040334.

[2] S. V. Dorozhkin, M. Epple, *Biological and Medical Significance of Calcium Phosphates. Angewandte Chemie − International Edition*, 2**002**. 41(17): p. 3130-3146, DOI: https://doi.org/10.1002/1521-3773(20020902)41:17<3130::AID-ANIE3130>3.0.CO;2-1.

[3] V. Sokolova, M. Epple, *Biological and Medical Applications of Calcium Phosphate Nanoparticles. Chemistry − A European Journal*, **2021**. 27(27): p. 7471-7488, DOI: https://doi.org/10.1002/chem.202005257.

[4] Y. Chen, Y. Feng, J. Deveaux, M. Masoud, F. Chandra, *Biomineralization Forming Process and Bio-inspired Nanomaterials for Biomedical Application: A Review*. Minerals **2019.** 9(68): p. 3-21, DOI: https://doi.org/10.3390/min9020068.

[5] Jeong, J. H. Kim, J. H. Shim, N. S. Hwang, C. Y. Heo*, Bioactive calcium phosphate materials and applications in bone regeneration*. Biomaterials Research, **2019**. 23(1): p. 4, DOI: 10.1186/s40824-018-0149-3.

[6] I. Antonia, *Handbook of Bioceramics and Biocomposites*. Springer, **2016.** 1(1): p. 35-91, DOI: https://doi.org/10.1007/978-3-319-12460-5.

[7] S. Dorozkin, *Calcium orthophosphates*. Biomatter, **2011**. 1(2): p. 121-164, DOI: https://doi.org/10.4161/biom.18790.

[8] G. MacLennan, C. Beevers, *The Crystal Structure of Monocalcium Phosphate Monohydrate*, **1956.** 9, p. 187-190, DOI: https://doi.org/10.1107/S0365110X56000413.

[9] A. C. Tas, *Transformation of Brushite (CaHPO$_4$·2H$_2$O) to Whitlockite (Ca$_9$Mg(HPO$_4$)(PO$_4$)$_6$) or Other CaPs in Physiologically Relevant Solutions*. Journal of the American Ceramic Society, **2016**. 99(4): p. 1200-1206, DOI: https://doi.org/10.1111/jace.14069.

[10] M. Landin, R.C. Rowe, P. York, *Structural changes during the dehydration of dicalcium phosphate dihydrate. European Journal of Pharmaceutical Sciences*, **1994**. 2(3): p. 245-252, DOI: https://doi.org/10.1016/0928-0987(94)90029-9.

[11] H. Zhou, L. Yang, U. Gbureck, S.B. Bhaduri, P. Sikder, *Monetite, an important calcium phosphate compound − Its synthesis, properties, and applications in orthopedics*. Acta Biomaterialia, **2021**. 127: p. 41-55, DOI: https://doi.org/10.1016/j.actbio.2021.03.050.

[12] O. Suzuki, *Evolution of octacalcium phosphate biomaterials*. Octacalcium Phosphate Biomaterials, **2020**. P. 1-15, DOI: https://doi.org/10.1016/B978-0-08-102511-6.00001-7.

[13] H. Lu, Y. Zhou, Y. Ma, *Current Application of Beta-Tricalcium Phosphate in Bone Repair and Its Mechanism to Regulate Osteogenesis*. Frontiers in Materials, **2021**. Multifunctional Bioactive Nanomaterials for Tissue Regeneration. 2: p. 1-10, DOI: https://doi.org/10.3389/fmats.2021.698915.

[14] R. Carrodeguas, S. De Aza, *α-Tricalcium phosphate: Synthesis, properties, and biomedical applications*. Acta Biomaterialia, **2011**. 7(10): p. 3536-3546, DOI: https://doi.org/10.1016/j.actbio.2011.06.019.

[15] G. Nancollas, M. LoRe, L. Perez, C. Richardson, S. J. Zawacki, *Mineral phases of calcium phosphate*. The Anatomical Record, **1989**. 224(2): 234-241, DOI: https://doi.org/10.1002/ar.1092240213.

[16] J. Mahamid, A. Sharir, L. Addabi, *Amorphous calcium phosphate as a major component of the forming fin bones of zebrafish: Indications for an amorphous precursor phase*. The Proceedings of the National Academy of Sciences, **2008**. 105(35): 12748-12753, DOI: https://doi.org/10.1073/pnas.0803354105.

[17] S. M. Barinov, *Calcium phosphate-based ceramic and composite materials for medicine.* Russian Chemical Reviews, **2010**. 79(1): p. 13-29, DOI: https://dx.doi.org/10.1070/RC2010v079n01ABEH004098.

[18] J. Kolmas, E. Groszyk, D. Kwiatkowska-Różycka, *Substituted hydroxyapatites with antibacterial properties.* BioMed research international, **2014**. 1(1): p. 178123-178123, DOI: https://doi.org/10.1155/2014/178123.

[19] V. G. Dileep Kumar, M. Santosh Sridhar, P. Aramwit, *A review on the synthesis and properties of hydroxyapatite for biomedical applications.* Journal of Biomaterials Science (Polymer Edition), **2022**. 33(2): p. 229-261, DOI: https://doi.org/10.1080/09205063.2021.1980985.

[20] C. Moseke, U. Gbureck, *Tetracalcium phosphate: Synthesis, properties, and biomedical applications.* Acta Biomaterialia, **2010**. 6(10): 3815-3823, DOI: https://doi.org/10.1016/j.actbio.2010.04.020.

[21] R. Lagier, C. A. Baud, *Magnesium Whitlockite, a Calcium Phosphate Crystal of Special Interest in Pathology.* Pathology - Research and Practice, **2003**. 199(5): p. 329-335, DOI: https://doi.org/10.1078/0344-0338-00425.

[22] M. Navarro, A. Michiardi, O. Castaño, L. A. Planell, *Biomaterials in orthopedics.* Journal of the Royal Society Interface, **2008**. 5(27): 1137-1158, DOI: https://doi.org/10.1098/rsif.2008.0151.

[23] T.C. Holmes, *Novel peptide-based biomaterial scaffolds for tissue engineering.* Trends in Biotechnology, **2002**. 20: p. 16–21, DOI: https:/10.1016/S0167-7799(01)01840-6.

[24] Z. Tang, X. Li, Y. Tan, H. Fan, X. Zhang, *The material and biological characteristics of osteoinductive calcium phosphates ceramics.* Regenerative Biomaterials, **2018**. 5(1): p. 43-59, DOI: https://doi.org/10.1093/rb/rbx024.

[25] T. T. Roberts, A. J. Rosenbaum, *Bone grafts, bone substitutes and orthobiologics.* Organogenesis, **2012**. 8(4) p. 114-124, DOI: https://doi.org/10.4161/org.23306.

[26] T. A Einhorn, C. A. Lee. *Bone regeneration: new findings and potential clinical applications.* Journal of the American Academy of Orthopaedic Surgeons, **2001**. 9: p. 157–65, DOI: https://doi.org/10.5435/00124635-200105000-00002.

[27] M. Šupová, *Substituted hydroxyapatites for biomedical applications: A review.* Ceramics International, **2015**. 41(8): p. 9203-9231, DOI: https://doi.org/10.1016/j.ceramint.2015.03.316.

[28] H. Xu, P. Wang, L. Wang, C. Bao, *Calcium phosphate cements for bone engineering and their biological properties*. Bone Research, **2017**. 5: p. 17056, DOI: https://10.1038/boneres.2017.56.

[29] E. Verron, I. Khairoun, J. Guicheux, J.-M. Bouler, *Calcium phosphate biomaterials as bone drug delivery systems: a review*. Drug Discovery Today, **2010**. 15(13): p. 547-552, DOI: https://doi.org/10.1016/j.drudis.2010.05.003.

[30] J. Raphel, M. Holodniy, S. B. Goodman, S. C. Heilshorn, *Multifunctional coatings to simultaneously promote osseointegration and prevent infection of orthopedic implants*. Biomaterials, **2016**. 84: p. 301-314, DOI: https://doi.org/10.1016/j.biomaterials.2016.01.016.

[31] M. Richards, J. A. Goylet, L. A. Weiss, N. A. Waanders, M. B. Schaffler, S. A. Goldstein, *Bone regeneration and fracture healing. Experience with distraction osteogenesis model*. Clinical Orthopaedics and Related Research, **1998**. 355: p. 191-204, PMID: 9917639.

[32] Y. Oshida, E. B. Tuna, O. Aktören, K. Gençay, *Dental Implant Systems*. International Journal of Molecular Sciences, **2010**. 11(4): p. 1580-1678, DOI: https://doi.org/10.3390/ijms11041580.

[33] T. J. Webster, E. A. Massa-Schlueter, J. L. Smith, E. B. Slamovich, *Osteoblast response to hydroxyapatite doped with divalent and trivalent cations*. Biomaterials, **2004**. 25(11): p. 2111-2121, DOI: https://doi.org/10.1016/j.biomaterials.2003.09.001.

[34] I. V. Fadeeva, M. R. Gafurov, I. A. Kiiaeva, S. B. Orlinskii, L. M. Kuznetsova, Y. Y. Filippov, A. S. Fomin, G. A. Davydova, I. I. Selezneva, S. M. Barinov, *Tricalcium Phosphate Ceramics Doped with Silver, Copper, Zinc, and Iron (III) Ions in Concentrations of Less Than 0.5 wt.% for Bone Tissue Regeneration*. BioNanoScience, **2017**. 7(2): p. 434-438, DOI: https://doi.org/10.1007/s12668-016-0386-7.

[35] E. Chang, G. Qin, *Antibacterial metals and alloys for potential biomedical implants*. Bioactive Materials, **2021**. 6(8): p. 2569-2612, DOI: https://doi.org/10.1016/j.bioactmat.2021.01.030.

[36] A. Bandyopadhyay, S. Bernard, W. Xue, S. Bose, *Calcium Phosphate-Based Resorbable Ceramics: Influence of MgO, ZnO, and SiO$_2$ Dopants*. Journal of the American Ceramic Society, **2006**. 89(9): p. 2675-2688, DOI: https://doi.org/10.1111/j.1551-2916.2006.01207.x.

[37] M. Munir, S. Salman, A. Ihsan, T. Elsaman, *Synthesis, Characterization, Functionalization, and Bio-Applications of Hydroxyapatite Nanomaterials: An Overview*. International Journal of Nanomedicine, **2022**. 17: p. 1903-1925, DOI: https://doi.org/10.2147/IJN.S360670.

[38] C. Kidney J., *Magnesium Basics*. Clinical Kidney Journal, **2012**. 5: p. 3-14, DOI: https://doi.org/10.1093/ndtplus/sfr163.

[39] G. K. Schwalfenberg, S. J. Genuis, *The Importance of Magnesium in Clinical Healthcare*. Scientifica, **2017**. 2017: p. 4179326, DOI: https://doi.org/10.1155/2017/4179326.

[40] N. E. L. Saris, E. Mervaala, H. Karppanen, *Magnesium: an update on physiological, clinical and analytical aspects*. Clinica Chimica Acta, **2000**. 294 (1-2):1–26, DOI: https://10.1016/S0009-8981(99)00258-2.

[41] M. Houston. *The role of magnesium in hypertension and cardiovascular disease*. Journal of Clinical Hypertension, **2011**. 13(11): p. 843–847, DOI: https://10.1111/j.1751-7176.2011.00538.x.

[42] U. Grober, J. Schmidt, K. Kisters, *Magnesium in prevention and therapy*. Nutrients, **2015**. 7(9): p. 8199–8226, DOI: https://10.3390/nu7095388.

[43] J. H. F. de Baaij, J. G. J. Hoenderop, R. J. M Bindels, *Magnesium in man: implications for health and disease*. Physiological Reviews, **2015**. 95(1): p. 1–46, DOI: https://10.1152/physrev.00012.2014.

[44] J. J. DiNicolantonio, J. H. O´Keefe, W. Wilson, *Subclinical magnesium deficiency: a principal driver of cardiovascular disease and a public health crisis.* Open Heart, **2018**. 5(1): 668, DOI: https://10.1136/openhrt-2017-000668.

[45] S. Castiglioni, A. Cazzaniga, W. Albisetti, J. A. M. Maier, *Magnesium, and Osteoporosis: Current State of Knowledge and Future Directions.* Nutrients, **2013**. 5(8): p. 3022-3033, DOI: https://10.3390/nu5083022.

[46] R. K. Rude, F. R. Singer, H. E Gruber, *Skeletal and hormonal effects of magnesium deficiency.* The Journal of the American College of Nutrition, **2009**. 28: p. 131–141. DOI: https://10.1080/07315724.2009.10719764.

[47] M. Aschner, Manganese. Advances in Nutirtion, **2017**. 8(3): p. 520-521, DOI: https://10.3945/an.117.015305.

[48] D. S. Avila, R. L. Puntel, M. Aschner, *Manganese in Health and Disease.* Metal ions in Life Sciences, **2013**. 13: p. 199-227, DOI: https://10.1007/978-94-007-7500-8_7.

[49] K. J. Horning, S. W. Caito, K.G, *Manganese is essential for neuronal health*. Annual Review of Nutrition, **2015**. 35: p. 71–108, DOI: https://10.1146/annurev-nutr-071714-034419.

[50] R. Lagier, C. A. Baud, *Magnesium Whitlockite, a Calcium Phosphate Crystal of Special Interest in Pathology.* Pathology - Research and Practice, **2003**. 199(5): p. 329-335, DOI: https://doi.org/10.1078/0344-0338-00425.

[51] H. L. Jang, K. Jin, J. Lee, Y. Kim, S. H. Nahm, K. S. Hong, K. T. Nam, *Revisiting Whitlockite, the Second Most Abundant Biomineral in Bone: Nanocrystal Synthesis in Physiologically Relevant Conditions and Biocompatibility Evaluation.* ACS Nano, **2014**. 8(1): p. 634-641, DOI: https://doi.org/10.1021/nn405246h.

[52] R. Gopal, C. Calvo, *Structural Relationship of Whitlockite and β-Ca$_3$(PO$_4$)$_2$.* Nature Physical Science, **1972**. 237(71): p. 30-32, DOI: https://doi.org/10.1038/physci237030a0.

[53] T. Debroise, E. Colombo, G. Belletti, J. Vekeman, Y. Su, R. Papoular, N. S. Hwang, D. Bazin, M. Daudon, P. Quaino, F. Tielens, *One Step Further in the Elucidation of the Crystallographic Structure of Whitlockite.* Crystal Growth & Design, **2020**. 20(4): p. 2553-2561, DOI: https://doi.org/10.1021/acs.cgd.9b01679.

[54] A. Kizalaitė, *Magnio ir Cinko Vitlokito Synthezė Tirpinimo-Nusodinimo Metodu,* **2020**. [Unpublished master's thesis]. Vilnius University.

[55] R. Gopal, C. Calvo, J. Ito, W. K. Sabine, *Crystal Structure of Synthetic Mg-Whitlockite, $Ca_{18}Mg_2H_2(PO_4)_{14}$.* Canadian Journal of Chemistry, **1974**. 52(7): p. 1155-1164, DOI: https://doi.org/10.1139/v74-181.

[56] H. D. Kim, H. L. Jang, H.-Y. Ahn, H. K. Lee, J. Park, E.-s. Lee, E. A. Lee, Y.-H. Jeong, D.-G. Kim, K. T. Nam, N. S. Hwang, *Biomimetic whitlockite inorganic nanoparticles-mediated in situ remodeling and rapid bone regeneration.* Biomaterials, **2017**. 112(1): p. 31-43, DOI: https://doi.org/10.1016/j.biomaterials.2016.10.009.

[57] C. Wang, K.-J. Jeong, H. J. Park, M. Lee, S.-C. Ryu, D. Y. Hwang, K. H. Nam, I. H. Han, J. Lee, *Synthesis and formation mechanism of bone mineral, whitlockite nanocrystals in the tri-solvent system.* Journal of Colloid and Interface Science, **2020**. 569(1): p. 1-11, DOI: https://doi.org/10.1016/j.jcis.2020.02.072.

[58] X. Guo, X. Liu, H. Gao, X. Shi, N. Zhao, Y. Wang, *Hydrothermal growth of whitlockite coating on β-tricalcium phosphate surfaces for enhancing bone repair potential.* Journal of Materials Science & Technology, **2018**. 34(6): p. 1054-1059, DOI: https://doi.org/10.1016/j.jmst.2017.07.009.

[59] C. Wang, K.-J. Jeong, H. J. Park, M. Lee, S.-C. Ryu, D. Y. Hwang, K. H. Nam, I. H. Han, J. Lee, *Synthesis and formation mechanism of bone mineral, whitlockite nanocrystals in the tri-solvent system.* Journal of Colloid and Interface Science, **2020**. 569(1): p. 1-11, DOI: https://doi.org/10.1016/j.jcis.2020.02.072.

[60] C. Lin, Y. Wang, Y. Zhou, Y. Zeng, *A rapid way to synthesize magnesium whitlockite microspheres for high efficiency removing heavy metals.* Desalination and Water Treatment, **2019**. 162(1): p. 220-227, DOI: https://doi.org/10.5004/dwt.2019.24290.

[61] L. Bauer, M. Ivanković, H. Ivanković. *Magnesium substituted hydroxyapatite scaffolds hydrothermally synthesized from cuttlefish bone*. MATRIB, **2018**. Vele Luka, Croatia.

SUMMARY

VILNIUS UNIVERSITY
FACULTY OF CHEMISTRY AND GEOSCIENCES

HANNA KLIPAN
Low-Temperature Synthesis and Characterization of Magnesium and Manganese Whitlockite

In the present work, magnesium and manganese whitlockite were synthesized by dissolution-precipitation process under hydrothermal conditions and low-temperature synthesis respectively. Synthesis conditions such as temperature, pH and reaction time were thoroughly studied and optimized.

It was demonstrated that pure-phase magnesium whitlockite can be synthesized hydrothermally in 3h at 160 °C, whereas pristine manganese whitlockite can be obtained by low-temperature synthesis at 75 °C at the same reaction time.

Thermal stability studies revealed that both magnesium and manganese are thermally unstable compounds and decomposed upon heat treatment with the formation of β-$Ca_3(PO_4)$, α-$Ca_2P_2O_7$, and β-$Ca_2P_2O_7$ phases.

Studies on magnetic properties demonstrated the paramagnetic nature of the synthesized manganese whitlockite both at 5 K and room temperatures.

Synthesized compounds were analyzed by X-ray diffraction and Rietveld refinement, Fourier-Transform Infrared and Raman spectroscopies, Scanning Electron Microscopy, Brunauer–Emmett–Teller (BET) surface area analysis. In addition, studies in magnetic properties and thermogravimetric measurements were performed

Therefore, cost-effective and rapid synthesis methods of magnesium and manganese whitlockite were developed. To the best of our knowledge, manganese whitlockite was synthesized for the first time in this work.